IEEE Access
Multidisciplinary | Rapid Review | Open Access Journal

Received November 1, 2019, accepted December 10, 2019, date of publication December 17, 2019,
date of current version January 17, 2020.

Digital Object Identifier 10.1109/ACCESS.2019.2960410

A Novel Fitting H-Infinity Kalman Filter for Nonlinear Uncertain Discrete-Time Systems Based on Fitting Transformation

JUAN XIA[1,2], SHESHENG GAO[2], YONGMIN ZHONG[3], JIAHAO ZHANG[2], CHENGFAN GU[3], AND YANG LIU[4]

[1]Research and Development Institute of Northwestern Polytechnical University in Shenzhen, Shenzhen 518057, China
[2]School of Automatics, Northwestern Polytechnical University, Xi'an 710072, China
[3]School of Engineering, RMIT University, Bundoora, VIC 3083, Australia
[4]China JIKAN Research Institute of Engineering Investigations and Design, Company, Ltd., Xi'an 710043, China

Corresponding author: Juan Xia (xiajuan_dr@ 163.com)

This work was supported in part by the National Nature Science Foundation of China under Grant 41704016, Grant 41804048, and Grant 41904028, in part by the Science, Technology and Innovation Commission of Shenzhen Municipality, China, under Grant JCYJ20180306171439979, and in part by the Shaanxi Province Key Research and Development Projects, China, under Grant 2018ZDXM-GY-024.

ABSTRACT The classical Kalman-based filtering algorithm, such as extended Kalman filter or unscented Kalman filter, commonly assumes that the accurate system model or precise noise statistics is known for using. Hence, these filters are not robust estimation to practical systems and always with poor stability, low precision or even divergence since uncertain items exist. In order to tackle these issues, a novel scheme referred to as the fitting H-infinity Kalman filter (FHKF) is proposed and used for robust estimation of the nonlinear uncertain systems. The hardcore of FHKF is the fitting transformation, which is a numerical approximation approach to get the estimation values of coefficient matrix based on least weighted squares. Moreover, FHKF is proposed by applying the coefficient matrix to the structure of the extended H-infinity Kalman filter. Based on the stochastic stability lemma, the stability analysis is presented to verify the error boundness of the proposed filtering. Its efficiency is demonstrated by taking Monte Carlo simulation for the uncertain system and practical experiments in the INS/GPS integrated navigation.

INDEX TERMS Fitting transformation, fitting H-infinity Kalman filter, stability analysis, uncertain system.

I. INTRODUCTION

The state estimation is an important research topic in many fields such as signal processing, target tracking, system identification, navigation and so on [1]–[3], [5], [6]. A large number of filtering approaches have been developed to address the problems of nonlinear state estimation [4].

From the perspective of the continuous-time systems, Taghvaei *et al.* introduced various modern extensions of the Kalman filter for the continuous-time nonlinear filtering problem [5]. Chen *et al.* [6], [7] designed the novel distributed formation controllers with estimating unknown parameters for the cases of the bidirectional or the directed strongly connected topology. For uncertain targets, redundant relative measurements are used to improve the robustness of the formation circumnavigation framework. This kind of estimation method makes high precision due to no rounding error, and it can be used for the continuous-time systems (i.e. in analog circuits). Meanwhile, generally speaking, it needs to be discretized in the engineering application generally.

From the perspective of the discrete-time system, nonlinear Kalman filters are commonly used such as the extended Kalman filter (EKF) [8], [9], unscented Kalman filter (UKF) [10], [11] and cubature Kalman filter (CKF) [12], [13]. This kind of filtering is assigned to the real-time recursion filtering, which does not need to store large amounts of measurement information in chronological order beforehand as the continuous-time filtering. Meanwhile, these filters require the prior statistics of random interference signals such as the process and measurement noises, which must be subject to the Gaussian distribution [14]. However, in practice, it is ubiquitous for a system to involve uncertainty, unknown noise

The associate editor coordinating the review of this manuscript and approving it for publication was Mohamed Kheir.

statistics, non-Gaussian noise or all of them [15]. If there is uncertainty involved in the dynamic system model, the above filters will lose the optimality, leading to deteriorated or diverged solutions [16].

Robust filtering methods were reported to solve the performance degradation involved in nonlinear Kalman-based filters [1], [17], [18]. The H∞ filter with H∞ norm as the performance standard is a robust filter for a variety of system uncertainties [4], [19]. It treats system modeling errors or uncertainties in the system as unknown but bounded noises, which is more flexible than the prior condition of noise statistics in Kalman-based filters. Different from Kalman-based filters which minimize the variance of estimation errors [4], the H∞ filter minimizes the effect of the worst-case disturbances on system state estimate. However, the H∞ filter is designed for linear systems, unsuitable for nonlinear systems [20].

Various improved H∞ filters were reported to address nonlinear filtering problems [21]–[24]. The extended H∞ Kalman filter (EHKF) is a commonly used method for nonlinear systems [25], [26]. It is an approximation filter using the linear Taylor (LT) approximation as the original nonlinear function. It is fast and easy to implement [26]. However, the using of LT causes a model error, which makes EHKF unsuitable for the cases that the nonlinear model is not derivable or the linearizable degree of a system is strong [20], [27]–[29]. Further, since LT is an approximation at one point, the using in EHKF to replace the entire random distribution area ignores the randomness of the system state, which affects the filtering accuracy. To overcome the EHKF problems, unscented transformation (UT) and spherical-radial cubature rules are applied to the structure of EHKF, leading to the unscented H∞ Kalman filter (UHKF) [29]–[31] and cubature H∞ Kalman filter (CHKF) [32], [33]. UHKF approximates the Gaussian integrals encountered in nonlinear filtering by a set of sample points determined by UT [30], while CHKF by a set of sample points determined according to spherical-radial cubature rules [33]. Both UHKF and CHKF can achieve not only high accuracy but also robustness under the disturbance of system error or uncertain noise. However, their improvements are achieved at the cost of expensive computations, especially for high-dimensional problems.

The fitting transformation (FT) [34] is a new numerical approximation method. According to the state distribution (typified by sample points), this method approximates a nonlinear system function by minimizing the error between the nonlinear function and a multivariate fitting function in the sense of weighted least squares (WLS). It has higher accuracy than LT approximation, especially for systems with strong nonlinearity. Similar to UT and spherical-radial cubature rules, FT also avoids the complex computation of the Jacobian matrix. Moreover, different from UT and spherical-radial cubature rules, FT provides a numerical FT matrix and thus it can be used for nonlinear systems without an analytical expression. Further, the principle of FT is also much simpler than those of UT and spherical-radial cubature rules. Therefore, FT provides a promising solution to address the EHKF problems due to the use of LT approximation. However, the incorporation of FT in the structure of EHKF is a difficult task and the related research has been very limited. Recently, Xiong *et al.* studied a linear fitting Kalman filter by applying FT into the structure of EKF [35]. As it inherits the basic theory of Kalman estimation solution, this method still suffers from the problems of Kalman-based filters. The fitting error is not considered in fitting system functions. Meanwhile, there is no theoretical proof of the relationship between FT and UT in [35].

This paper presents a novel fitting H-infinity Kalman filter (FHKF) for nonlinear filtering based on numerical approximation with a low computational cost. Instead of LT, this filter applies FT to the structure of EHKF. Specifically, the **main contributions** of this paper are as following:

1) The novel FT is presented based on the improvement of the original FT in [34]. According to the pre-obtained sample sets, the new fitting function and fitting matrices are created by FT even without the analytical expression. Meanwhile, the relationship between FT and UT is established by theoretical analysis, which rigorously derives that FT has a similar approximation accuracy as UT. However, it does not need to select the unknown parameter like UT.
2) FHKF is proposed as a robust estimation approach based on FT technique with a low computational cost. It takes into account the minimization of the approximation error as a posterior distribution function of the system state. It not only avoids complex computations, but also provides a numerical Jacobian matrix, and thus it can also be used for nonlinear systems without an analytical expression. The proposed FHKF is also robust to system uncertainties due to the use of the upper bound. Meanwhile, the attenuation level γ_o, which is used to improve the overall performance in the estimation process is adaptively estimated in FHKF. We design an adaptive relevant parameter to ensure the asymptotic optimality of attenuation level, which indicates the asymptotically optimal upper bound of filtering. Moreover, there is no redundant parameter selection in filtering design.
3) The stability analysis of FHKF is presented as a theoretical method according to the stochastic stability lemma. It indicates that the filtering solution of the proposed method is bounded and stable even if the attenuation level $\gamma_o \to \infty$. Furthermore, the simulation experiments and comparison analysis demonstrate the improved performance of the proposed FHKF.

II. FITTING TRANSFORMATION

The system state $\boldsymbol{x}$ is a column vector of $n \times 1$. According to linear fitting [34], [35], the state function of the nonlinear

system can be expressed as

$$z = g(x) = Ax + b + e = \tilde{A}\tilde{x} + e \tag{1}$$

where z is a vector of $m\times 1$, $\mathbf{A}$ is a coefficient matrix of $m\times n$, b is a constant vector of $m\times 1$, and e represents the linearization error. $\tilde{\mathbf{A}}$ and $\tilde{x}$ are expressed by

$$\tilde{\mathbf{A}} = \begin{bmatrix} \mathbf{A} & b \end{bmatrix}_{m\times(n+1)} = [\tilde{a}_1^T, \tilde{a}_2^T, \cdots, \tilde{a}_m^T]^T \tag{2}$$

$$\tilde{x} = [x^T \quad 1]^T \tag{3}$$

where $\tilde{\mathbf{A}}$ is a matrix of $m \times (n+1)$, and $\tilde{x}$ is a vector of $(n+1)\times 1$.

By WLS [34], the linear fitting parameters of $g(x)$ are determined as

$$\hat{\tilde{\mathbf{A}}} = \arg\min_{\tilde{A}} [g(x) - \tilde{\mathbf{A}}\tilde{x}]^T \mathbf{W}[*] \tag{4}$$

where $\mathbf{W}$ is the positive weighting matrix.

It should be noted that it is difficult to find an analytical solution to (4). In the following, we shall discuss how to use FT to solve (4).

Assume that the mean and covariance are $\tilde{x}_{00}$ and P_{00} for a set of sample points which represents the probability distribution of x. Weight the set of sample points by

$$[\tilde{\mathbf{X}}, \ \mathbf{W}] = \mathbf{sp}\left[\tilde{x}_{00}, P_{00}\right] \tag{5}$$

where $\tilde{\mathbf{X}} = \begin{bmatrix} x_{00} \pm \sqrt{\mathbf{P}_{00}}\xi \\ \mathbf{1}_{1\times 2n} \end{bmatrix}$, $\mathbf{W} = \frac{1}{2n}\mathbf{I}_{2n}$, the unit points are $\xi = [\sqrt{n}\mathbf{I}_n, -\sqrt{n}\mathbf{I}_n]$, and $\mathbf{1}_{1\times 2n}$ represents a $1 \times 2n$ vector with all elements as 1.

Substituting all sample points $\tilde{\mathbf{X}}$ into (1) yields

$$\mathbf{Z}^T = \tilde{\mathbf{X}}^T\tilde{\mathbf{A}}^T + \mathbf{E}^T \tag{6}$$

where

$$\tilde{\mathbf{X}} = \begin{bmatrix} \tilde{x}_1 & \tilde{x}_2 \cdots \tilde{x}_{2n} \end{bmatrix} \tag{7}$$

$$\mathbf{E} = [e_1, e_2, \cdots, e_{2n}] = [\tilde{e}_1^T, \tilde{e}_2^T, \cdots, \tilde{e}_m^T]^T \tag{8}$$

$$\mathbf{Z} = [f(\tilde{x}_1), f(\tilde{x}_2), \cdots, f(\tilde{x}_{2n})] = [\tilde{z}_1^T, \tilde{z}_2^T, \cdots, \tilde{z}_m^T]^T \tag{9}$$

and $\tilde{\mathbf{X}}$ is the $(n+1)\times 2n$ matrix consisting of sample points, $\mathbf{E} \in \mathbf{R}^{m\times 2n}$ is the linearization error of all the sample points, and the j-th column of $\mathbf{Z}^T$ is

$$\tilde{z}_j^T = \tilde{\mathbf{X}}_j^T\tilde{a}_j^T + \tilde{e}_j^T \tag{10}$$

where $\tilde{e}_j$ is a vector related to all the sample points and $j = 1, \cdots, m$. Then, the minimization problem described by (4) can be solved by estimating the parameter $\tilde{a}_j$ to minimize the error $\tilde{e}_j$ in terms of WLS

$$\hat{\tilde{a}}_j^T = (\tilde{\mathbf{X}}W\tilde{\mathbf{X}}^T)^{-1}\tilde{\mathbf{X}}W\tilde{z}_j^T = (\tilde{\mathbf{X}}\tilde{\mathbf{X}}^T)^{-1}\tilde{\mathbf{X}}\tilde{z}_j^T \tag{11}$$

where $\mathbf{W} = diag([w_1, w_2, \cdots, w_{2n}])$.

Finally, estimate the fitting matrix $\tilde{\mathbf{A}}$ and the fitting error covariance $\mathbf{P}_{ee}$ by WLS

$$\hat{\tilde{\mathbf{A}}} = [(\tilde{X}\tilde{X}^T)^{-1}\tilde{X}Z^T]^T \tag{12}$$

$$\mathbf{P}_{ee} = [\mathbf{Z} - \hat{\tilde{\mathbf{A}}}\tilde{X}_i]\mathbf{W}[*]^T \tag{13}$$

TABLE 1. FT algorithm.

Input: $f(\cdot)$, $\tilde{x}_{00} \in \mathbf{R}^{(n+1)\times 1}$, and $P_{00} \in \mathbf{R}^{n\times n}$

Output: $\hat{\tilde{A}}$ and $\mathbf{P}_{ee}$

1. By (5), generate the sample set $\tilde{X} \in \mathbf{R}^{(n+1)\times 2n}$ and its weight coefficients matrix is $\mathbf{W} \in \mathbf{R}^{2n\times 2n}$.
2. Substitute the sample points $\tilde{X}$ into $f(\cdot)$ to obtain the matrix $\mathbf{Z}$.
3. Calculate the fitting matrix $\tilde{A}$ and the fitting error covariance $\mathbf{P}_{ee}$ by (12) and (13).

* where $\mathbf{R}^{n\times m}$ indicates a matrix of $n \times m$.

Table 1 shows the detailed algorithm of a novel FT, which is considering the error in fitting system functions.

Remark 1: Theorem 1 reveals that FT has the same approximation accuracy as UT. The sampling sets $\{\tilde{\mathbf{X}}, \mathbf{Z}\}$ in FT can be generated in two different ways. One is that the sampling set is created by the rules in (5) at each time step based on the spherical cubature rule with the specific analytical expression (It is mainly used in this article owing to its simplicity). The other is that the sampling sets of inputs and outputs are gotten by multiple training without the analytical expression. It provides basic thinking of establishing mathematical models of unknown system. According to the pre-obtained sample sets and the basic idea of regression, the new fitting dynamic function and fitting matrices are created by FT even without the analytical expression and applied to the next robust filtering. However, the sample set in UT cannot be obtained without the analytical expression since its criteria are different from FT.

Remark 2: It is the parameter κ selected in advance that determines the performance of unscented filters [4], [30]. The best parameter entirely depends on the specific circumstances of the subject. The inappropriate parameter can cause the poor performance of filtering [4]. Moreover, it is worth noting that the filtering could be interrupted due to the non-positive covariance in UT. Nevertheless, there are no such issues in FT, which does not need the selection of unknown parameters. Due to no redundant calculation, it can be implemented with a lower complex computation.

Theorem 1: Consider a nonlinear function $z = g(x)$ with mean x_{00} and covariance P_{00}. The accuracy to approximate $g(x)$ by FT is the same as that by UT.

Proof: The proof is described in Appendix B.

III. FITTING H-INFINITY KALMAN FILTER

Since LT is an approximation at one point and then using it replace the entire random distribution area. The randomness of states which affects the filtering precision is ignored in EHKF. Moreover, the performance of UHKF is related to the selection of unknown parameters. The filtering is interrupted due to the non-positive covariance in UT. Meanwhile, the computational complexity is relatively large with the above redundant computing. The sample-set in UHKF cannot be obtained without the known analytical expression. Thus, to address the above issues, FT is designed based on the idea of regression or fitting that avoids selecting unknown

parameters. The nonlinear dynamic function is fitted by the pre-obtained sampling sets even without specific analytical expression. It can be implemented with a lower complex computation as well.

However, some difficulties in the design of FHKF present as follows. i) The selection of sampling number and sample set. ii) Integrating FT into the structure of nonlinear H-infinity based filtering to obtain FHKF by considering the covariance $\mathbf{P}_{ee}$ of fitting errors. iii) Verifying the estimated error boundness of the proposed FHKF is work worth considering. These difficulties can be overcome in this section and the next section.

A. THE NONLINEAR SYSTEM AND ITS APPROXIMATION

Consider the discrete-time nonlinear dynamic state-space model

$$\begin{cases} \boldsymbol{x}_k = \boldsymbol{f}(\boldsymbol{x}_{k-1}) + \boldsymbol{w}_k \\ \boldsymbol{z}_k = \boldsymbol{h}(\boldsymbol{x}_k) + \boldsymbol{v}_k \end{cases} \tag{14}$$

where $\boldsymbol{f}(\cdot)$ and $\boldsymbol{h}(\cdot)$ denote the non-linear process and measurement function; $\boldsymbol{x}_k \in \mathbf{R}^n$ is the n-dimensional state; $\boldsymbol{z}_k \in \mathbf{R}^m$ is the measurement; $\boldsymbol{w}_k$ is the process noise with non-zero mean and unknown or deterministic variance $\mathbf{Q}_k$ as well as bounded energy, i.e., $\sum_{k=0}^{\infty} \boldsymbol{w}_k^T \boldsymbol{w}_k < \infty$; and v_k is the measurement noise with non-zero mean and unknown or deterministic variance $\mathbf{R}_k$ as well as bounded energy, i.e., $\sum_{k=0}^{\infty} \boldsymbol{v}_k^T \boldsymbol{v}_k < \infty$. $\boldsymbol{w}_k$ and $\boldsymbol{v}_k$ are assumed to be uncorrelated.

The estimation error can be written as

$$\Delta \boldsymbol{x}_k \triangleq \boldsymbol{x}_k - \hat{\boldsymbol{x}}_k \tag{15}$$

Let $J(\upsilon)$ represent the transfer operator to map the unknown disturbances $\boldsymbol{x}_0 - \hat{\boldsymbol{x}}_0$, $\{\boldsymbol{w}_j\}_{j=0}^k$ and $\{\boldsymbol{v}_j\}_{j=0}^k$ to the estimation error $\{\Delta \boldsymbol{x}_j\}_{j=0}^k$, where $\hat{\boldsymbol{x}}_0$ is the priority estimation of $\boldsymbol{x}_0$, and $\boldsymbol{x}_0 - \hat{\boldsymbol{x}}_0$ indicates the unknown estimation error. The nonlinear H∞ filter aims to select an appropriate strategy υ to minimize $\Delta \boldsymbol{x}_j$.

Define $\|\boldsymbol{f}\|_{\mathbf{S}}^2 = \boldsymbol{f}^T \mathbf{S} \boldsymbol{f}, \quad \forall \boldsymbol{f} \in \mathbf{R}^n$, where $\mathbf{S}$ is an asymmetric and positive definite matrix. The standard transfer operator (i.e., the cost function) of H∞ norm is represented by

$$J_k = \sup_{x_0, w, v \in l_2} \frac{\sum_{j=0}^{k} \|\Delta x_j\|_2^2}{\|x_0 - \hat{x}_0\|_{\mathbf{P}_0^{-1}}^2 + \sum_{j=0}^{k} (\|w_j\|_{\mathbf{Q}^{-1}}^2 + \|v_j\|_{\mathbf{R}^{-1}}^2)} \tag{16}$$

where $J_k < \gamma_o^2$, $\gamma_o > 0$ is the attenuation level specified by users, and $\mathbf{P}_0$ is the covariance of the state estimation error at the initial time. Applying FT to (14) yields

$$\begin{cases} \boldsymbol{x}_k = \hat{\boldsymbol{\Phi}}_{k-1} \hat{\boldsymbol{x}}_{k-1} + \boldsymbol{u}_{x,k-1} + \boldsymbol{e}_{x,k-1} + \boldsymbol{w}_{k-1} \\ = \hat{\tilde{\boldsymbol{\Phi}}}_{k-1} \hat{\tilde{\boldsymbol{x}}}_{k-1} + \boldsymbol{e}_{x,k-1} + \boldsymbol{w}_{k-1} \\ \boldsymbol{z}_k = \hat{\mathbf{H}}_k \hat{\boldsymbol{x}}_{k/k-1} + \boldsymbol{u}_{z,k-1} + \boldsymbol{e}_{z,k-1} + \boldsymbol{v}_k \\ = \hat{\tilde{\boldsymbol{H}}}_k \hat{\tilde{\boldsymbol{x}}}_{k/k-1} + \boldsymbol{e}_{z,k-1} + \boldsymbol{v}_k \end{cases} \tag{17}$$

where $\hat{\tilde{\boldsymbol{x}}}_{k-1} = [\hat{\boldsymbol{x}}_{k-1}^T, 1]^T$; $\hat{\tilde{\boldsymbol{x}}}_{k/k-1} = [\hat{\boldsymbol{x}}_{k/k-1}^T, 1]^T$; $\boldsymbol{u}_{x,k-1}$ and $\boldsymbol{u}_{z,k-1}$ are the constant fitting terms of the process and measurement functions; $\boldsymbol{e}_{x,k-1}$ and $\boldsymbol{e}_{z,k-1}$ are the fitting errors of the process function; and $\hat{\tilde{\boldsymbol{\Phi}}}_{k-1}$ and $\hat{\tilde{\boldsymbol{H}}}_k$ are the fitting matrices of $\boldsymbol{f}(\cdot)$ and $\boldsymbol{h}(\cdot)$, which are represented as according to (4)

$$\begin{cases} \hat{\tilde{\boldsymbol{\Phi}}}_{k-1} = \arg\min_{\tilde{A}} \boldsymbol{e}_{x,k-1}^T \mathbf{W}_{x,k-1} \boldsymbol{e}_{x,k-1} \\ = \arg\min_{\tilde{\boldsymbol{\Phi}}_{k-1}} [\boldsymbol{f}(\boldsymbol{x}_{k-1}) - \tilde{\boldsymbol{\Phi}}_{k-1} \hat{\tilde{\boldsymbol{x}}}_{k-1}]^T \mathbf{W}_{x,k-1} [*] \\ \hat{\tilde{\boldsymbol{H}}}_k = \arg\min_{\tilde{A}} \boldsymbol{e}_{z,k-1}^T \mathbf{W}_{z,k} \boldsymbol{e}_{z,k-1} \\ = \arg\min_{\tilde{\mathbf{H}}_k} [\boldsymbol{h}(\boldsymbol{x}_{k/k-1}) - \tilde{\boldsymbol{H}}_k \hat{\tilde{\boldsymbol{x}}}_{k/k-1}]^T \mathbf{W}_{z,k} [*] \end{cases} \tag{18}$$

B. DERIVATION OF FITTING H-INFINITY KALMAN FILTER

Applying FT to the structure of EHKF [25] yields

$$\hat{\tilde{\boldsymbol{x}}}_{k-1} = [\hat{\boldsymbol{x}}_{k-1}^T \ \ 1]^T \tag{19}$$

$$[\hat{\tilde{\boldsymbol{\Phi}}}_{k-1}, \mathbf{P}_{k-1,xe}] \leftarrow \mathrm{FT}(\boldsymbol{f}(\cdot), \hat{\tilde{\boldsymbol{x}}}_{k-1}, \mathbf{P}_{k-1}) \tag{20}$$

$$\hat{\tilde{\boldsymbol{x}}}_{k/k-1} = \hat{\tilde{\boldsymbol{\Phi}}}_{k-1} \hat{\tilde{\boldsymbol{x}}}_{k-1} \tag{21}$$

$$\mathbf{P}_{k/k-1} = \hat{\boldsymbol{\Phi}}_{k-1} \mathbf{P}_{k-1} \hat{\boldsymbol{\Phi}}_{k-1}^T + \mathbf{Q}_{k,o} \tag{22}$$

$$[\hat{\boldsymbol{H}}_k, \mathbf{P}_{k/k-1,ze}] \leftarrow \mathrm{FT}(\boldsymbol{h}(\cdot), \hat{\tilde{\boldsymbol{x}}}_{k/k-1}, \mathbf{P}_{k/k-1}) \tag{23}$$

$$\mathbf{K}_k = \mathbf{P}_{k/k-1} \hat{\mathbf{H}}_k^T (\mathbf{R}_{k,o} + \hat{\mathbf{H}}_k \mathbf{P}_{k/k-1} \hat{\mathbf{H}}_k^T)^{-1} \tag{24}$$

$$\hat{\boldsymbol{x}}_k = \hat{\tilde{\boldsymbol{x}}}_{k/k-1} + \mathbf{K}_k (\boldsymbol{z}_k - \hat{\boldsymbol{H}}_k \hat{\boldsymbol{x}}_{k/k-1}) \tag{25}$$

$$\mathbf{P}_k = \mathbf{P}_{k/k-1} - \mathbf{P}_{k/k-1} [-\mathbf{I}_n^T \ \hat{\mathbf{H}}_k^T] \mathbf{M}_k^{-1} [-\mathbf{I}_n^T \ \hat{\mathbf{H}}_k^T]^T \mathbf{P}_{k/k-1} \tag{26}$$

$$\mathbf{M}_k = \begin{bmatrix} -\gamma_o^{-2} \mathbf{I}_n & \mathbf{0} \\ \mathbf{0} & \mathbf{R}_{k,o}^{-1} \end{bmatrix} + [-\mathbf{I}_n^T \ \hat{\mathbf{H}}_k^T]^T \mathbf{P}_{k/k-1} [-\mathbf{I}_n^T \ \hat{\mathbf{H}}_k^T] \tag{27}$$

where $\mathbf{P}_{k-1,xe}$ is the covariance of $\boldsymbol{e}_{x,k-1}$; $\hat{\boldsymbol{\Phi}}_{k-1}$ is the numerical Jacobian matrix of $\boldsymbol{f}(\cdot)$, which is the fitting matrix $\hat{\tilde{\boldsymbol{\Phi}}}_{k-1}$ without the last column; $\mathbf{P}_{k/k-1,ze}$ is the covariance of $\boldsymbol{e}_{z,k-1}$; $\mathbf{K}_k$ is the gain matrix of the state vector; $\mathbf{Q}_{k,o} = \mathbf{P}_{k-1,xe} + \mathbf{Q}_k$ and $\mathbf{R}_{k,o} = \mathbf{R}_k + \mathbf{P}_{k/k-1,ze}$. By the matrix inversion lemma, (26) can be further written as

$$\mathbf{P}_k^{-1} = \mathbf{P}_{k/k-1}^{-1} + \hat{\mathbf{H}}_k^T \mathbf{R}_{k,o}^{-1} \hat{\mathbf{H}}_k - \gamma_o^{-2} \mathbf{I}_n > 0 \tag{28}$$

where γ_o is the attenuation level to adjust the filtering robustness and accuracy and is determined according to (16); and $\hat{\mathbf{H}}_k$ is the numerical Jacobian matrix of $\boldsymbol{h}(\cdot)$, which is the fitting matrix $\hat{\boldsymbol{H}}_k$ without the last column.

The attenuation level γ_o has an important influence on the filtering performance. For the traditional H∞ filter, it is a known value which is generally determined by the experience of engineering practices. To solve above problem, adaptive adjustment of γ_o is presented for improving the filtering performance. According to lemma in [22], the existence condition (28) can be obtained as

$$\gamma_o^2 > \lambda((\mathbf{P}_{k/k-1}^{-1} + \hat{\mathbf{H}}_k^T \mathbf{R}_{k,o}^{-1} \hat{\mathbf{H}}_k)^{-1}) \tag{29}$$

where $\lambda(\mathbf{A})$ denotes the maximum eigenvalue of $\mathbf{A}$. According to (22), it can be written as

$$\hat{\gamma}_{o,k} = \eta_k \sqrt{\lambda((\mathbf{P}_{k/k-1}^{-1} + \hat{\mathbf{H}}_k^T \mathbf{R}_{k,o}^{-1} \hat{\mathbf{H}}_k)^{-1})} \tag{30}$$

where $\hat{\gamma}_{o,k}$ is the local minimum for the attenuation level γ_o and $\eta_k = 1 + \eta_{k-1}^{-1} (\eta_0 > 0)$.

Remark 3: The attenuation level γ_o^2 is the upper bound of H-infinity norm of estimation error, and its local minimum at time k is $\hat{\gamma}_{o,k}$. The smaller fixed-γ_o causes instability and unavailability of filtering. In contrast, the larger fixed γ_o could cause poor robust, which takes large estimation errors. Its adaptive adjustment is aimed to estimate the optimal upper at each instant time to improve the robustness, stability, and availability. However, there is no absolute optimal upper bound for H-infinity based filters by (30). Therefore, we design an adaptive relevant parameter η_k to ensure the asymptotic optimality of $\hat{\gamma}_{o,k}$, which tends to the optimal upper bound asymptotically. Meanwhile, it is designed by decreasing adaptively to achieve the absolute convergence of local attenuation level, which promises better performance. The related parameter η_k is decreased over time to increase the robustness and availability of filtering process. Thus, the min-max criteria is used by the proposed filtering to bound these uncertainties without online tuning of them.

C. ALGORITHM IMPLEMENTATION

The proposed FHKF includes the following steps:

Step 1: Initialize the state and its covariance: $\hat{\boldsymbol{x}}_0 = \boldsymbol{x}_0$ and $\mathbf{P}_0 = \varepsilon \mathbf{I}_n$, where $\mathbf{I}_n$ is the n-dimensional unit matrix.

Step 2: Update the state parameters by (19)-(20) based on FT.

Step 3: Prediction update: update the prediction mean $\hat{\tilde{\boldsymbol{x}}}_{k/k-1}$ and the prediction covariance $\mathbf{P}_{k/k-1}$ by (21)-(22).

Step 4. Update the measurement parameters by (23) based on FT.

Step 5: Update the attenuation level $\hat{\gamma}_{o,k}$ by (30).

Step 6: Measurement update: update the state estimation $\hat{\boldsymbol{x}}_k$ and the covariance $\mathbf{P}_k$ by (24)-(25), (26)-(27) or (28).

Remark 4: For the selected sampling number or set, too few sample points could lead to poor precision, and too many points could result in computational redundancy. The sample points are selected symmetrically to obtain a fitting function with superior performance. It is undoubtedly that the optimal choice is not only characterize the sampling distribution but also present superior performance. Then, FT is integrated into the structure of H-infinity based filters to design FHKF. The fitting model of nonlinear system is established by fitting transformation to get the fitting matrices, which are combined with H-infinity based filtering. Moreover, the covariance of fitting errors is considered and used to compensate for fitting errors in filtering.

Remark 5: As FT′s inherited the characteristics, unlike unscented filters, the selection of important unknown parameter values is unnecessary for FHKF. The attenuation level about the optimal upper bound in FHKF as an important parameter is adaptively estimated according to the specific rules in (30), and then FHKF is a robust filter based on the adaptive parameter. The asymptotically optimal bound is designed to guarantee better robustness and availability. Hence, by using the adaptive upper bound at each instant time, the estimation performance is under control with the situation of system uncertainties. Due to no redundant calculation, it can be implemented with a lower complex computation.

Remark 6: The prerequisite of the FHKF filtering, i.e., $J_k < \gamma_o^2$ described by (16), is that the estimation error $\Delta \boldsymbol{x}_k$ is bounded. When $\gamma_o \to \infty$, it will be the same as the linear fitting Kalman filter (see Appendix A for details).

Proof: The proof is described in Appendix B.

IV. STOCHASTIC STABILITY OF FITTING H-INFINITY KALMAN FILTER

In order to verify the estimated error boundness of the proposed FHKF, the stochastic stability analysis as a theoretical method is considered in this section. Analysis result indicates that the filtering solution of the proposed method is bounded and stable even if the attenuation level tends to infinity. For a large value γ_o^2 or even $\gamma_o^2 \to \infty$, the cost function J_k has a large upper bound or even no upper bound. Then the estimation error increases, which leads to a poor or even divergence solution. Therefore, it is necessary to analyze the stability of FHKF, especially when $\gamma_o^2 \to \infty$. Since a large upper bound is a special case of $\gamma_o^2 \to \infty$, without loss of generality, we only discuss the filtering stability for $\gamma_o^2 \to \infty$.

Lemma 1 [10], [36, [37]: Suppose that there is a random process $V(\xi_k)$ as well as real numbers $v_{\min} > 0$, $v_{\max} > 0$, $\mu > 0$ and $0 < \lambda \leqslant 1$, such that the following inequalities hold

$$v_{\min} ||\xi_k||^2 \leqslant V(\xi_k) \leqslant v_{\max} ||\xi_k||^2 \tag{31}$$

$$E\left[V(\xi_k)|\xi_{k-1}\right] - V(\xi_{k-1}) \leqslant \mu - \lambda V(\xi_{k-1}) \tag{32}$$

Then, the root mean square (RMS) of the random process ξ_k is bounded, i.e.

$$E\left\{||\xi_k||^2\right\} \leqslant \frac{v_{\max}}{v_{\min}} E\left\{||\xi_0||^2\right\} (1-\lambda)^k + \frac{\mu}{v_{\min}} \sum_{i=1}^{k-1} (1-\lambda)^i \tag{33}$$

where the operator $||\cdot||$ is the Euclidean norm in $\mathbf{R}^n$.

Define the prediction error as

$$\Delta \boldsymbol{x}_{k/k-1} = \boldsymbol{x}_k - \hat{\boldsymbol{x}}_{k/k-1} \tag{34}$$

By (14), (21) and (22), the prediction error vector can be calculated as

$$\begin{aligned} \Delta \boldsymbol{x}_{k/k-1} &= f(x_{k-1}) - \hat{\tilde{\boldsymbol{\Phi}}}_k \hat{\tilde{\boldsymbol{x}}}_k + \boldsymbol{w}_k \\ &= \hat{\tilde{\boldsymbol{\Phi}}}_k \tilde{\boldsymbol{x}}_k + \boldsymbol{e}_{k,x} - \hat{\tilde{\boldsymbol{\Phi}}}_k \hat{\tilde{\boldsymbol{x}}}_k + \boldsymbol{w}_k \\ &= \hat{\tilde{\boldsymbol{\Phi}}}_k (\tilde{\boldsymbol{x}}_k - \hat{\tilde{\boldsymbol{x}}}_k) + \boldsymbol{e}_{k,x} + \boldsymbol{w}_k \\ &\approx \hat{\boldsymbol{\Phi}}_k \Delta \boldsymbol{x}_{k-1} + \boldsymbol{w}_k \end{aligned} \tag{35}$$

where $\Delta \boldsymbol{x}_k = \boldsymbol{x}_k - \hat{\boldsymbol{x}}_k$ is the estimation error. Similarly, the innovation $\Delta \boldsymbol{z}_k$ can be calculated as

$$\begin{aligned}\Delta \boldsymbol{z}_k &= \boldsymbol{z}_k - \hat{\boldsymbol{z}}_k \\ &= \boldsymbol{h}(\boldsymbol{x}_{k/k-1}) - \hat{\hat{\mathbf{H}}}_k \hat{\tilde{\boldsymbol{x}}}_{k/k-1} + \boldsymbol{v}_k \\ &= \hat{\hat{\mathbf{H}}}_k \tilde{\boldsymbol{x}}_{k/k-1} + \boldsymbol{e}_{k/k-1,z} - \hat{\hat{\mathbf{H}}}_k \hat{\tilde{\boldsymbol{x}}}_{k/k-1} + \boldsymbol{v}_k \\ &= \hat{\hat{\mathbf{H}}}_k (\tilde{\boldsymbol{x}}_{k/k-1} - \hat{\tilde{\boldsymbol{x}}}_{k/k-1}) + \boldsymbol{e}_{k/k-1,z} + \boldsymbol{v}_k \\ &\approx \hat{\mathbf{H}}_k \Delta \boldsymbol{x}_{k/k-1} + \boldsymbol{v}_k \end{aligned} \tag{36}$$

Then, the prediction error $\Delta \boldsymbol{x}_{k|k-1}$ and the innovation $\Delta \boldsymbol{z}_k$ can be expressed as

$$\Delta \boldsymbol{x}_{k/k-1} = \boldsymbol{\beta}_k \hat{\boldsymbol{\Phi}}_k \Delta \boldsymbol{x}_{k-1} + \boldsymbol{w}_k \tag{37}$$

$$\Delta \boldsymbol{z}_k = \boldsymbol{\theta}_k \hat{\mathbf{H}}_k \Delta \boldsymbol{x}_{k/k-1} + \boldsymbol{v}_k \tag{38}$$

where $\boldsymbol{\beta}_k$ and $\boldsymbol{\theta}_k$ are the unknown diagonal matrices at time k. Suppose that $\boldsymbol{e}_{k,x}$ is not related to $\Delta \boldsymbol{x}_{k-1}$, from (35) the covariance of the prediction error vector is

$$\begin{aligned}&E(\Delta \boldsymbol{x}_{k/k-1} \Delta \boldsymbol{x}_{k/k-1}^T) \\ &= E[(\hat{\boldsymbol{\Phi}}_k \Delta \boldsymbol{x}_{k-1} + \boldsymbol{e}_{k,x} + \boldsymbol{w}_k)(*)^T] \\ &= \hat{\boldsymbol{\Phi}}_k \mathbf{P}_{k-1} \hat{\boldsymbol{\Phi}}_k^T + \mathbf{P}_{k-1,xe} + \mathbf{Q} + \delta \mathbf{P}_{k/k-1} \\ &= \hat{\boldsymbol{\Phi}}_k \mathbf{P}_{k-1} \hat{\boldsymbol{\Phi}}_k^T + \mathbf{Q}_{k,o} + \delta \mathbf{P}_{k/k-1} \end{aligned} \tag{39}$$

From (37), the covariance of the prediction error vector is written as

$$\begin{aligned}&E(\Delta \boldsymbol{x}_{k/k-1} \Delta \boldsymbol{x}_{k/k-1}^T) \\ &= E[(\boldsymbol{\beta}_k \hat{\boldsymbol{\Phi}}_k \Delta \boldsymbol{x}_{k-1} + \boldsymbol{w}_k)(*)^T] \\ &= (\boldsymbol{\beta}_k \hat{\boldsymbol{\Phi}}_k) \mathbf{P}_{k-1} (*)^T + \mathbf{Q} + \boldsymbol{\beta}_k \delta \mathbf{P}_{k/k-1} \end{aligned} \tag{40}$$

For simplicity, denote

$$\mathbf{A}_k = \boldsymbol{\beta}_k \hat{\boldsymbol{\Phi}}_k, \ \mathbf{B}_k = \boldsymbol{\theta}_k \hat{\mathbf{H}}_k, \ \mathbf{C}_k = \mathbf{I} - \mathbf{K}_k \mathbf{B}_k \tag{41}$$

Since (39) and (40) are equivalent and considering (21) and (22), the prediction error covariance can be written as

$$\mathbf{P}_{k/k-1} = \mathbf{A}_k \mathbf{P}_{k-1} \mathbf{A}_k^T + \mathbf{Q}_{k,e} \tag{42}$$

where $\mathbf{Q}_{k,e} = [\mathbf{Q} + (\boldsymbol{\beta}_k - \mathbf{I}) \delta \mathbf{P}_{k/k-1}]$.

Since $\gamma_o^2 \to \infty$ means $\gamma_o^{-2} \to 0$, (28) can be further written as

$$\begin{aligned}\mathbf{P}_k^{-1} &= \mathbf{P}_{k/k-1}^{-1} + \hat{\mathbf{H}}_k^T \mathbf{R}_{k,o}^{-1} \hat{\mathbf{H}}_k - \gamma_o^{-2} \mathbf{I}_n \\ &= \mathbf{P}_{k/k-1}^{-1} + \hat{\mathbf{H}}_k^T \mathbf{R}_{k,o}^{-1} \hat{\mathbf{H}}_k \end{aligned} \tag{43}$$

Substituting (43) into (24), the gain matrix is obtained as

$$\begin{aligned}\mathbf{K}_k &= (\mathbf{P}_{k/k-1}^{-1} + \hat{\mathbf{H}}_k^T \mathbf{R}_{k,o}^{-1} \hat{\mathbf{H}}_k^T)^{-1} \hat{\mathbf{H}}_k^T \mathbf{R}_{k,o}^{-1} \\ &= \mathbf{P}_k \hat{\mathbf{H}}_k^T \mathbf{R}_{k,o}^{-1} \end{aligned} \tag{44}$$

Substituting (14) and (25) into $\Delta \boldsymbol{x}_k = \boldsymbol{x}_k - \hat{\boldsymbol{x}}_k$ yields

$$\begin{aligned}\Delta \boldsymbol{x}_k &= \Delta \boldsymbol{x}_{k/k-1} - \mathbf{K}_k \Delta \boldsymbol{z}_k \\ &= \mathbf{A}_k \Delta \boldsymbol{x}_{k-1} + \boldsymbol{w}_k - \mathbf{K}_k (\mathbf{B}_k \Delta \boldsymbol{x}_{k/k-1} + \boldsymbol{v}_k) \\ &= \mathbf{A}_k \Delta \boldsymbol{x}_{k-1} + \boldsymbol{w}_k - \mathbf{K}_k \mathbf{B}_k \mathbf{A}_k \Delta \boldsymbol{x}_{k-1} \\ &\quad - \mathbf{B}_k \boldsymbol{w}_k - \mathbf{K}_k \boldsymbol{v}_k \\ &= \mathbf{C}_k \mathbf{A}_k \Delta \boldsymbol{x}_{k-1} + \mathbf{C}_k \boldsymbol{w}_k - \mathbf{K}_k \boldsymbol{v}_k \end{aligned} \tag{45}$$

Theorem 2: Consider the random dynamic system described by (14), when $\gamma_o^2 \to \infty$, if the following conditions are fulfilled:

$$\begin{aligned}a_{\min} \mathbf{I} \leqslant \mathbf{A}_k \mathbf{A}_k^T \leqslant a_{\max} \mathbf{I}, \ \mathbf{B}_k \mathbf{B}_k^T \leqslant b_{\max} \mathbf{I} \\ \mathbf{C}_k \mathbf{C}_k^T \leqslant c_{\max} \mathbf{I}, \ h_{\min} \mathbf{I} \leqslant \hat{\mathbf{H}}_k \hat{\mathbf{H}}_k^T \leqslant h_{\max} \mathbf{I} \end{aligned} \tag{46}$$

are held for any positive real numbers $a_{\min}$, $a_{\max}$, $b_{\max}$ and $c_{\max}$;

$$\begin{aligned}\mathbf{R} \leqslant r_{\max} \mathbf{I}, \ q_{\min} \leqslant \mathbf{Q} \leqslant q_{\max} \mathbf{I}, \ p_{\min} \mathbf{I} \leqslant \mathbf{P}_k \leqslant p_{\max} \mathbf{I} \\ r_{o,\min} \mathbf{I} \leqslant \mathbf{R}_{k,o}, \ q_{e,\min} \mathbf{I} < \mathbf{Q}_{k,e} \leqslant q_{e,\max} \mathbf{I} \end{aligned} \tag{47}$$

are held for any positive real numbers $q_{\max}$, $q_{\min}$, $p_{\min}$, $p_{\max}$, $r_{o,\min}$, $r_{o,\max}$, $q_{o,\min}$and $q_{o,\max}$, where $r_{o,\min} > b_{\max}(p_{\max} a_{\max} + q_{\max}) - h_{\min}(p_{\min} a_{\min} + q_{\min})$; and for any real number $\varepsilon_{\max} > 0$, we have

$$\left\| \hat{\mathbf{H}}_k - \mathbf{B}_k \right\| \leqslant \varepsilon_{\max} \tag{48}$$

where $\varepsilon_{\max}^2 < a_{\max}^{-1} (p_{\max} + p_{\max}^2 a_{\max} q_{\min}^{-1})^{-1} r_{o,min}$.

Then, the estimation error $\Delta \boldsymbol{x}_k$ is bounded in the mean square even when the cost function is unbounded, i.e., $\gamma_o^2 \to \infty$. In other words, FHKF is always stable as long as $\gamma_o^2 > 0$.

Proof: Define the Lyapunov function as

$$V_k(\Delta \boldsymbol{x}_k) = \Delta \boldsymbol{x}_k^T \mathbf{P}_k^{-1} \Delta \boldsymbol{x}_k \tag{49}$$

According to (31), the bounds of the Lyapunov function are obtained as

$$\frac{1}{p_{\max}} ||\Delta x_k||^2 \leqslant V_k(\Delta x_k) \leqslant \frac{1}{p_{\min}} ||\Delta x_k||^2 \tag{50}$$

In order to fulfill the conditions in **Lemma 1**, the upper bound of $E[\Delta \boldsymbol{x}_k | \Delta \boldsymbol{x}_{k-1}] - V(\Delta \boldsymbol{x}_{k-1})$ in (32) needs to be found. Substituting (45) into (49), $V_k(\Delta \boldsymbol{x}_k)$ can be represented as

$$V_k(\Delta \boldsymbol{x}_k) = (\mathbf{C}_k \mathbf{A}_k \Delta \boldsymbol{x}_{k-1} + \mathbf{C}_k \boldsymbol{w}_k - \mathbf{K}_k \boldsymbol{v}_k)^T \mathbf{P}_k^{-1} (*) \tag{51}$$

Thus, the conditional expectation can be written as

$$\begin{aligned}&E[V_k(\Delta \boldsymbol{x}_k) | \Delta \boldsymbol{x}_{k-1}] \\ &= E[(\mathbf{C}_k \mathbf{A}_k \Delta \boldsymbol{x}_{k-1} + \mathbf{C}_k \boldsymbol{w}_k - \mathbf{K}_k \boldsymbol{v}_k)^T \mathbf{P}_k^{-1} (*) | \Delta \boldsymbol{x}_{k-1}] \\ &= E[(\mathbf{C}_k \mathbf{A}_k \Delta \boldsymbol{x}_{k-1})^T \mathbf{P}_k^{-1} (*) + (\mathbf{C}_k \boldsymbol{w}_k)^T \mathbf{P}_k^{-1} (*) \\ &\quad + (\mathbf{K}_k \boldsymbol{v}_k)^T \mathbf{P}_k^{-1} (*) | \Delta \boldsymbol{x}_{k-1}] \\ &= E[(\Delta \boldsymbol{x}_{k-1}^T \mathbf{A}_k^T \mathbf{C}_k^T \mathbf{P}_k^{-1} \mathbf{C}_k \mathbf{A}_k \Delta \boldsymbol{x}_{k-1} \\ &\quad + \boldsymbol{w}_k^T \mathbf{C}_k^T \mathbf{P}_k^{-1} \mathbf{C}_k \boldsymbol{w}_k + \boldsymbol{v}_k^T \mathbf{K}_k^T \mathbf{P}_k^{-1} \mathbf{K}_k \boldsymbol{v}_k) | \Delta \boldsymbol{x}_{k-1}] \end{aligned} \tag{52}$$

Substituting (33), (46) and (47) into the first item of (52), we get

$$\begin{aligned}
&E[\Delta \boldsymbol{x}_{k-1}^T \mathbf{A}_k^T \mathbf{C}_k^T \mathbf{P}_k^{-1} \mathbf{C}_k \mathbf{A}_k \Delta \boldsymbol{x}_{k-1} | \Delta \boldsymbol{x}_{k-1}] \\
&\quad = E[\Delta \boldsymbol{x}_{k-1}^T \mathbf{A}_k^T (\mathbf{I} - \mathbf{B}_k^T \mathbf{K}_k^T) \mathbf{P}_k^{-1} (\mathbf{I} - \mathbf{K}_k \mathbf{B}_k) \\
&\qquad \cdot \mathbf{A}_k \Delta \boldsymbol{x}_{k-1} | \Delta \boldsymbol{x}_{k-1}] \\
&\quad = E[\Delta \boldsymbol{x}_{k-1}^T (\mathbf{A}_k^T \mathbf{P}_k^{-1} \mathbf{A}_k - \mathbf{A}_k^T \mathbf{B}_k^T \mathbf{K}_k^T \mathbf{P}_k^{-1} \mathbf{A}_k \\
&\qquad - \mathbf{A}_k^T \mathbf{P}_k^{-1} \mathbf{K}_k \mathbf{B}_k \mathbf{A}_k + \mathbf{A}_k^T \mathbf{B}_k^T \mathbf{K}_k^T \mathbf{P}_k^{-1} \mathbf{K}_k \mathbf{B}_k \mathbf{A}_k) \\
&\qquad \cdot \Delta \boldsymbol{x}_{k-1} | \Delta \boldsymbol{x}_{k-1}] \\
&\quad = \Delta \boldsymbol{x}_{k-1}^T \mathbf{A}_k^T \mathbf{P}_{k/k-1}^{-1} \mathbf{A}_k \Delta \boldsymbol{x}_{k-1} + (\mathbf{A}_k \Delta \boldsymbol{x}_{k-1})^T \\
&\qquad \cdot (\hat{\mathbf{H}}_k^T \mathbf{R}_{k,o}^{-1} \hat{\mathbf{H}}_k - \mathbf{B}_k^T \mathbf{R}_{k,o}^{-1} \hat{\mathbf{H}}_k - \hat{\mathbf{H}}_k^T \mathbf{R}_{k,o}^{-1} \mathbf{B}_k \\
&\qquad + \mathbf{B}_k^T \mathbf{R}_{k,o}^{-1} \hat{\mathbf{H}}_k \mathbf{P}_k \hat{\mathbf{H}}_k^T \mathbf{R}_{k,o}^{-1} \mathbf{B}_k)(*)
\end{aligned} \tag{53}$$

where

$$\begin{aligned}
\mathbf{B}_k^T \mathbf{R}_{k,o}^{-1} \hat{\mathbf{H}}_k \mathbf{P}_k \hat{\mathbf{H}}_k^T \mathbf{R}_{k,o}^{-1} \mathbf{B}_k = \mathbf{B}_k^T [\mathbf{R}_{k,o}^{-1} \\
- (\hat{\mathbf{H}}_k \mathbf{P}_{k/k-1} \hat{\mathbf{H}}_k^T + \mathbf{R}_{k,o})^{-1}] \mathbf{B}_k
\end{aligned} \tag{54}$$

Letting $\boldsymbol{\mu_k} = E(\boldsymbol{w}_k^T \mathbf{C}_k^T \mathbf{P}_k^{-1} \mathbf{C}_k \boldsymbol{w}_k + \boldsymbol{v}_k^T \mathbf{K}_k^T \mathbf{P}_k^{-1} \mathbf{K}_k \boldsymbol{v}_k)$ and considering (53) and (54), (52) can be expanded as

$$\begin{aligned}
&E[V_k(\Delta \boldsymbol{x}_k) | \Delta \boldsymbol{x}_{k-1}] \\
&\quad = \Delta \boldsymbol{x}_{k-1}^T \mathbf{A}_k^T \mathbf{P}_{k/k-1}^{-1} \mathbf{A}_k \Delta \boldsymbol{x}_{k-1} + (\mathbf{A}_k \Delta \boldsymbol{x}_{k-1})^T \\
&\qquad \cdot (\hat{\mathbf{H}}_k^T \mathbf{R}_{k,o}^{-1} \hat{\mathbf{H}}_k - \mathbf{B}_k^T \mathbf{R}_{k,o}^{-1} \hat{\mathbf{H}}_k - \hat{\mathbf{H}}_k^T \mathbf{R}_{k,o}^{-1} \mathbf{B}_k \\
&\qquad + \mathbf{B}_k^T \mathbf{R}_{k,o}^{-1} \hat{\mathbf{H}}_k \mathbf{P}_k \hat{\mathbf{H}}_k^T \mathbf{R}_{k,o}^{-1} \mathbf{B}_k)(*) + \mu_k \\
&\quad = \Delta \boldsymbol{x}_{k-1}^T \mathbf{A}_k^T \mathbf{P}_{k/k-1}^{-1} \mathbf{A}_k \Delta \boldsymbol{x}_{k-1} + (\mathbf{A}_k \Delta \boldsymbol{x}_{k-1})^T \\
&\qquad \cdot \{\hat{\mathbf{H}}_k^T \mathbf{R}_{k,o}^{-1} \hat{\mathbf{H}}_k - \mathbf{B}_k^T \mathbf{R}_{k,o}^{-1} \hat{\mathbf{H}}_k - \hat{\mathbf{H}}_k^T \mathbf{R}_{k,o}^{-1} \mathbf{B}_k \\
&\qquad + \mathbf{B}_k^T [\mathbf{R}_{k,o}^{-1} - (\hat{\mathbf{H}}_k \mathbf{P}_{k/k-1} \hat{\mathbf{H}}_k^T + \mathbf{R}_{k,o})^{-1}] \mathbf{B}_k\}(*) \\
&\qquad + \mu_k \\
&\quad = \Delta \boldsymbol{x}_{k-1}^T \mathbf{A}_k^T \mathbf{P}_{k/k-1}^{-1} \mathbf{A}_k \Delta \boldsymbol{x}_{k-1} + (\mathbf{A}_k \Delta \boldsymbol{x}_{k-1})^T \\
&\qquad \cdot [(\hat{\mathbf{H}}_k - \mathbf{B}_k)^T \mathbf{R}_{k,o}^{-1} (*) - \mathbf{B}_k^T (\hat{\mathbf{H}}_k \mathbf{P}_{k/k-1} \hat{\mathbf{H}}_k^T + \mathbf{R}_{k,o})^{-1} \\
&\qquad \cdot \mathbf{B}_k](*) + \mu_k
\end{aligned} \tag{55}$$

Subtracting $V_{k-1}(\Delta \boldsymbol{x}_{k-1})$ from both sides of (55) yields

$$\begin{aligned}
&E[V_k(\Delta \boldsymbol{x}_k) | \Delta \boldsymbol{x}_{k-1}] - V_{k-1}(\Delta \boldsymbol{x}_{k-1}) \\
&\quad = \Delta \boldsymbol{x}_{k-1}^T \mathbf{A}_k^T (\mathbf{A}_k \mathbf{P}_{k-1} \mathbf{A}_k^T + \mathbf{Q}_{k,e})^{-1} \mathbf{A}_k \Delta \boldsymbol{x}_{k-1} \\
&\qquad - \Delta \boldsymbol{x}_{k-1}^T \mathbf{P}_{k-1}^{-1} \mathbf{A}_k \Delta \boldsymbol{x}_{k-1} \\
&\qquad + (\mathbf{A}_k \Delta \boldsymbol{x}_{k-1})^T [(\hat{\mathbf{H}}_k - \mathbf{B}_k)^T \mathbf{R}_{k,o}^{-1} (\hat{\mathbf{H}}_k - \mathbf{B}_k) \\
&\qquad - \mathbf{B}_k^T (\hat{\mathbf{H}}_k \mathbf{P}_{k/k-1} \hat{\mathbf{H}}_k^T + \mathbf{R}_{k,o})^{-1} \mathbf{B}_k](*) + \mu_k \\
&\quad = \Delta \boldsymbol{x}_{k-1}^T [\mathbf{A}_k^T (\hat{\mathbf{H}}_k - \mathbf{B}_k)^T \mathbf{R}_{k,o}^{-1} (\hat{\mathbf{H}}_k - \mathbf{B}_k) \mathbf{A}_k \\
&\qquad - \mathbf{A}_k^T \mathbf{B}_k^T (\hat{\mathbf{H}}_k \mathbf{P}_{k/k-1} \hat{\mathbf{H}}_k^T + \mathbf{R}_{k,o})^{-1} \mathbf{B}_k \mathbf{A}_k \\
&\qquad - (\mathbf{P}_{k-1} + \mathbf{P}_{k-1} \mathbf{A}_k^T \mathbf{Q}_{k,e}^{-1} \mathbf{A}_k \mathbf{P}_{k-1})^{-1}](*) + \mu_k
\end{aligned} \tag{56}$$

Then, a form similar to (37) can be written as

$$\begin{aligned}
&E[V_k(\Delta \boldsymbol{x}_k) | \Delta \boldsymbol{x}_{k-1}] - V_{k-1}(\Delta \boldsymbol{x}_{k-1}) \\
&\quad = \mu_k - \lambda_k V_{k-1}(\Delta \boldsymbol{x}_{k-1})
\end{aligned} \tag{57}$$

where

$$\begin{aligned}
\lambda_k = \Delta \boldsymbol{x}_{k-1}^T [&-\mathbf{A}_k^T (\hat{\mathbf{H}}_k - \mathbf{B}_k)^T \mathbf{R}_{k,o}^{-1} (\hat{\mathbf{H}}_k - \mathbf{B}_k) \mathbf{A}_k \\
&+ \mathbf{A}_k^T \mathbf{B}_k^T (\hat{\mathbf{H}}_k \mathbf{P}_{k/k-1} \hat{\mathbf{H}}_k^T + \mathbf{R}_{k,o})^{-1} \mathbf{B}_k \mathbf{A}_k \\
&+ (\mathbf{P}_{k-1} + \mathbf{P}_{k-1} \mathbf{A}_k^T \mathbf{Q}_{k,e}^{-1} \mathbf{A}_k \mathbf{P}_{k-1})^{-1}] \\
&\cdot (*) / V_{k-1}(\Delta \boldsymbol{x}_{k-1})
\end{aligned} \tag{58}$$

Now let us determine the ranges of μ_k and λ_k. Substituting (44) and taking the trace on both sides of μ_k yield

$$\begin{aligned}
\mu_k &= E[trace(\boldsymbol{w}_k^T \mathbf{C}_k^T \mathbf{P}_k^{-1} \mathbf{C}_k \boldsymbol{w}_k + \boldsymbol{v}_k^T \mathbf{K}_k^T \mathbf{P}_k^{-1} \mathbf{K}_k \boldsymbol{v}_k)] \\
&= E[trace(\boldsymbol{w}_k^T \mathbf{C}_k^T \mathbf{P}_k^{-1} \mathbf{C}_k \boldsymbol{w}_k \\
&\quad + \boldsymbol{v}_k^T \mathbf{R}_{k,o}^{-1} \hat{\mathbf{H}}_k \mathbf{P}_k \hat{\mathbf{H}}_k^T \mathbf{R}_{k,o}^{-1} \boldsymbol{v}_k)]
\end{aligned} \tag{59}$$

Thus, μ_k can be represented as

$$\mu_k = trace[(\mathbf{C}_k^T \mathbf{P}_k^{-1} \mathbf{C}_k) \mathbf{Q}_k + (\mathbf{R}_{k,o}^{-1} \hat{\mathbf{H}}_k \mathbf{P}_k \hat{\mathbf{H}}_k^T \mathbf{R}_{k,o}^{-1}) \mathbf{R}] \tag{60}$$

Applying the matrix identity $tr(AB) = tr(BA)$ and considering (46) and (47), we have

$$\begin{aligned}
\mu_k &\leqslant c_{\max}^2 p_{\min}^{-1} q_{\max} L + r_{\mathrm{o,min}}^{-2} h_{\max} p_{\max} r_{\max} M \\
&\triangleq \mu_{\max}
\end{aligned} \tag{61}$$

Choosing $\mu_{\max} > 0$, (61) becomes

$$\mu_k \leqslant \mu_{\max} \tag{62}$$

Based on (46)-(48), the second term of (60) satisfies the following condition

$$\Delta \boldsymbol{x}_{k-1}^T \mathbf{A}_k^T \mathbf{B}_k^T (\hat{\mathbf{H}}_k \mathbf{P}_{k/k-1} \hat{\mathbf{H}}_k^T + \mathbf{R}_{k,o})^{-1} \mathbf{B}_k \mathbf{A}_k \Delta \boldsymbol{x}_{k-1} \geqslant 0 \tag{63}$$

Let

$$\begin{aligned}
\tau_k = \Delta \boldsymbol{x}_{k-1}^T [&-\mathbf{A}_k^T (\hat{\mathbf{H}}_k - \mathbf{B}_k)^T \mathbf{R}_{k,o}^{-1} (\hat{\mathbf{H}}_k - \mathbf{B}_k) \mathbf{A}_k \\
&+ (\mathbf{P}_{k-1} + \mathbf{P}_{k-1} \mathbf{A}_k^T \mathbf{Q}_{k,e}^{-1} \mathbf{A}_k \mathbf{P}_{k-1})^{-1}] \Delta \boldsymbol{x}_{k-1}
\end{aligned} \tag{64}$$

where

$$\begin{aligned}
\tau_k > [&-a_{\max} \varepsilon_{\max}^2 r_{o,min}^{-1} + (p_{\max} + p_{\max}^2 a_{\max} q_{e,\min}^{-1})^{-1}] \\
&\Delta x_{k-1}^T \Delta x_{k-1} \triangleq \tau_{\min} \geqslant 0
\end{aligned} \tag{65}$$

From (58) and (63)-(65), it can be verified that

$$\lambda_k V_{k-1}(\Delta \boldsymbol{x}_{k-1}) > \tau_k > \tau_{\min} \tag{66}$$

Then, it follows from (66) that

$$\lambda_k V_{k-1}(\Delta \boldsymbol{x}_{k-1}) > 0, \quad or \ \lambda_k > 0 \tag{67}$$

where the value on the right of (67) denotes the upper bound of λ_k or $\lambda_k V_{k-1}(\Delta \boldsymbol{x}_{k-1})$.

Let

$$\begin{aligned}
&(\mathbf{P}_{k-1} + \mathbf{P}_{k-1} \mathbf{A}_k^T \mathbf{Q}_{k,e}^{-1} \mathbf{A}_k \mathbf{P}_{k-1})^{-1} - \mathbf{P}_{k-1}^{-1} \\
&\quad = -\mathbf{A}_k^T (\mathbf{A}_k \mathbf{P}_{k-1} \mathbf{A}_k^T + \mathbf{Q}_{k,e})^{-1} \mathbf{A}_k
\end{aligned} \tag{68}$$

$$-\Delta x_{k-1}^T \mathbf{A}_k^T (\hat{\mathbf{H}}_k - \mathbf{B}_k)^T \mathbf{R}_{k,o}^{-1} (\hat{\mathbf{H}}_k - \mathbf{B}_k) \mathbf{A}_k \Delta \boldsymbol{x}_{k-1} \leqslant 0 \tag{69}$$

By (46)-(48), we can obtain

$$\begin{aligned}&\lambda_k V_{k-1}(\Delta x_{k-1}) - V_{k-1}(\Delta x_{k-1})\\ &\leqslant \Big(\frac{a_{\max} b_{\max}}{(p_{\min} a_{\min} + q_{\min}) h_{\min} + r_{o,\min}}\\ &\quad - \frac{a_{\max}}{p_{\max} a_{\max} + q_{\max}} \Big) \Delta x_{k-1}^T (*) \end{aligned} \tag{70}$$

Obviously, we can obtain the lower bound

$$\lambda_k V_{k-1}(\Delta \boldsymbol{x}_{k-1}) - V_{k-1}(\Delta \boldsymbol{x}_{k-1}) < 0, \quad or\ \lambda_k < 1 \tag{71}$$

From (67) and (71), the upper bound of λ_k can be obtained as

$$\lambda_{\min} = \min_k(\lambda_k) \in (0, 1) \tag{72}$$

Therefore, applying **Lemma 1**, (62) and (72), (57) can be satisfied by

$$\begin{aligned}E[V_k(\Delta \boldsymbol{x}_k)|\Delta \boldsymbol{x}_{k-1}] - V_{k-1}(\Delta \boldsymbol{x}_{k-1}) &\leqslant \mu_{\max}\\ &\quad - \lambda_{\min} V_{k-1}(\Delta \boldsymbol{x}_{k-1})\end{aligned} \tag{73}$$

Equation (73) indicates (33) is fulfilled. It also guarantees the boundness of the estimation error $\Delta \boldsymbol{x}_k$ when $\gamma_o^2 \to \infty$. Thus, FHKF is stable when $\gamma_o^2 > 0$. The proof of Theorem 2 is completed.

V. PERFORMANCE EVALUATION AND DISCUSSION

The performance of the proposed FHKF was evaluated by two simulation cases. Firstly, the comparison of the accuracy of mean and covariance between FT with LT and UT by using on the 2D transformation from the Polar coordinate system to the Cartesian coordinate system. Secondly, the reentry vehicle tracking system is being used to compare the presence of system noises between FHKF with UKF, EHKF, and UHKF.

A. TRANSFORMATION FROM POLAR TO CARTESIAN COORDINATE SYSTEM

In sensor-related problems, the polar coordinate (r, θ) is commonly used to characterize the target′s dynamics. However, the physical world is most commonly described by the Cartesian coordinate system. Therefore, it is necessary to transform the polar coordinate system (r, θ) into the Cartesian coordinate system. Consider the 2D transformation from the polar coordinate (r, θ) to the Cartesian coordinate system (x, y)

$$z = \begin{pmatrix} x \\ y \end{pmatrix} = \begin{pmatrix} r\cos\theta \\ r\sin\theta \end{pmatrix} \tag{74}$$

Suppose the real position is (0, 1), the standard deviation of the range and bearing measurement are $2cm$ and 15°, respectively. The parameter κ in UT is set to $(\alpha^2 - 1)n$ by multi-test, where $\alpha = 0.1$. Meanwhile, the target in the polar coordinate follows the Gaussian distribution. The mean and covariance of the position vector z in the Cartesian coordinate system are calculated by Monte-Carlo stochastic sampling and taken as the reference data to assess the approximation accuracy. Fig. 1 shows the samples in the Cartesian coordinate system by 2000 Monte-Carlo simulations. Define the 1σ contour by $\{z : (z - \hat{z})\mathbf{P}_{zz}^{-1}(z - \hat{z})^T = 1\}$ [38].

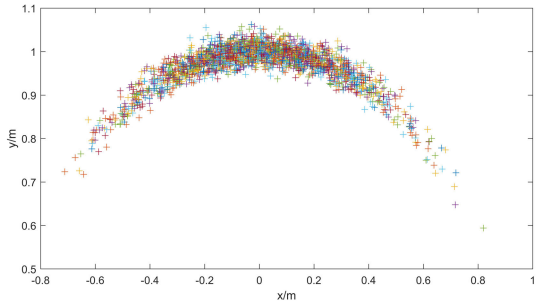

FIGURE 1. The simulated samples from the coordinate transformation.

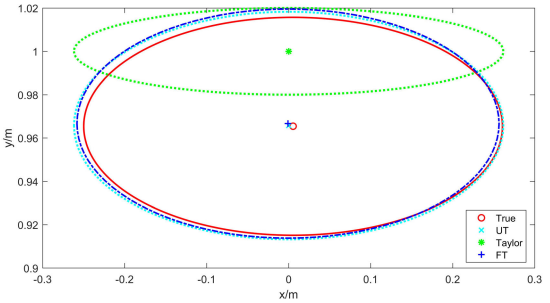

FIGURE 2. The means and standard deviation contours of z by LT, UT and FT. The true values of mean and standard deviation are indicated by the circle symbol and red ellipse. The UT mean and standard deviation are displayed by the cross symbol and cyan ellipse. The LT mean and standard deviation are displayed by star symbol and green ellipse. The FT mean and standard deviation are displayed by the plus symbol and blue ellipse.

TABLE 2. The mean and standard deviations of by LT, UT and FT.

	Means(mm)		standard deviations(mm)	
	x	y	x	y
true	**5.4**	**965.4**	**254.3**	**50.6**
LT	0	1000	264.8	20.43
UT	5.65	965.7	253.8	51.9
FT	**5.78**	**965.6**	**257.4**	**51.5**

The approximations of the position vector z by FT, UT, and LT are shown in Fig. 2. Their specific means and standard deviations are shown in Table 2. The means of both FT and UT are extremely close to the reference mean, and their errors are within $10^{-5}m$. The standard deviations of both FT and UT are also within $10^{-3}m$. In contrast, the errors between the mean and standard deviation of LT and the real values are $(5.40 \times 10^{-3}m,\ \ 0.0346m)$ and $(0.0105m,\ \ 0.0302m)$, respectively. Thus, it is evident that LT is significantly inferior than the accuracy of FT and UT. Both FT and UT have a similar accuracy, which is much better than that of LT and also in agreement with Theorem 1. However, the select of the parameters in UT is hard work as stated in remark 2. The filtering could be interrupted by the non-positive covariance in UT.

B. THE REENTRY VEHICLE TRACKING SYSTEM

Simulation trials were conducted to evaluate the performance of the proposed FHKF for a reentry vehicle tracking system,

which is a typical nonlinear problem. Consider that a vehicle enters the atmosphere at a high altitude with a high velocity. The position of the vehicle is tracked by radar to measure the distance and bearing angle of the vehicle. The system model is same as (14) and the states vector is defined as

$$\boldsymbol{x}(t) = [x_1, x_2, x_3, x_4, x_5]^T \tag{75}$$

where (x_1, x_2) and (x_3, x_4) denote the position and velocity of the vehicle, and denotes the aerodynamic parameter (aero-param).

The nonlinear process function is defined as

$$\begin{aligned}\dot{\boldsymbol{x}}(t) &= \boldsymbol{f}(\boldsymbol{x}(t)) + \boldsymbol{w}(t) \\ &= \begin{bmatrix} x_3(t) \\ x_4(t) \\ D(t)x_3(t) + G(t)x_1(t) \\ D(t)x_4(t) + G(t)x_2(t) \\ 0 \end{bmatrix} + \boldsymbol{w}(t)\end{aligned} \tag{76}$$

where $D(t) = \beta(t)exp\left[(R_0 - R(t))/H_0\right]V(t)$ is the drag-related force term, $G(t) = GM_0/R^3(t)$ is the gravity-related force term, and $\beta(t) = \beta_0 \exp(x_5(t))$, where $R(t) = \sqrt{x_1^2(t) + x_2^2(t)}$ is the distance from Earth's core to the vehicle and $V(t) = \sqrt{x_3^2(t) + x_4^2(t)}$ is the total speed. R_0, H_0, β_0 and GM_0 are constants as $R_0 = 6374$, $H_0 = 13.406$, $\beta_0 = -0.59783$, $GM_0 = 3.986 \times 10^5$.

The reference variances of $\boldsymbol{w}(t)$ is

$$\mathbf{Q} = \text{diag}([10^{-6}, 10^{-6}, 10^{-4}, 10^{-4}, 10^{-6}])$$

The measurement vector is

$$z_k = [d_k, \theta_k] \tag{77}$$

where d_k is the distance between the vehicle and radar, and θ_k is the bearing angle of the vehicle. The nonlinear measurement function is

$$\begin{aligned}z_k &= \boldsymbol{h}(\boldsymbol{x}_k) + \boldsymbol{v}_k \\ &= \begin{bmatrix} \sqrt{(x_1(t) - x_s)^2 + (x_2(t) - y_s)^2} \\ \tan^{-1}[(x_2(t) - y_s)/(x_2(t) - x_s)] \end{bmatrix} + \boldsymbol{v}_k\end{aligned} \tag{78}$$

where (x_s, y_s) denotes the location of the radar. The reference variances of $\boldsymbol{v}_k$ is

$$\mathbf{R} = \text{diag}([(10^{-3})^2; (0.17 \times 10^{-3})^2])$$

Fig. 3 shows a sample trajectory of the vehicle with respect to earth and radar. For comparison analysis, simulation trials were conducted by UKF, EHKF [25], UHKF [30], adaptive UKF (AUKF) [39] and FHKF under the same conditions, i.e., the parameters are set as

$$\gamma_{ehkf}^2 = 10, \quad \eta_{uhkf} = \eta_0^{fhkf} = 4$$

the initial state estimate and its covariance are

$$\begin{aligned}\hat{\boldsymbol{x}}_0 &= [6500.4,\ 349.14,\ -1.80,\ 6.79,\ 0.69] \\ \hat{\mathbf{P}}_0 &= \text{diag}([1, 1, 1, 1, 0.1])\end{aligned}$$

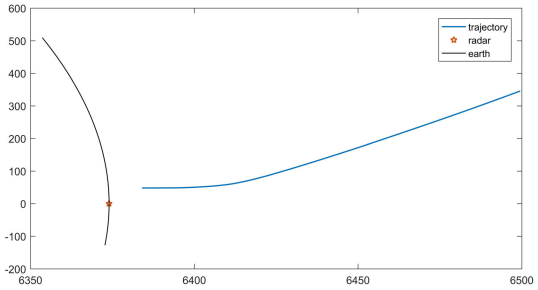

FIGURE 3. The trajectory of the simulation system.

The root mean square errors (RMSEs) of position and velocity are selected as the performance metrics in this paper. It is defined at time t as

$$\begin{aligned}&RMSE_{pos}(t) \\ &= \sqrt{\frac{1}{M}\sum_{i=1}^{M}\left[x_1^i(t) - \hat{x}_1^i(t)\right]^2 + \left[x_2^i(t) - \hat{x}_2^i(t)\right]^2}\end{aligned} \tag{79}$$

where $\left(x_1^i(t), x_2^i(t)\right)$ and $\left(\hat{x}_1^i(t), \hat{x}_2^i(t)\right)$ represent the real and estimated position, respectively, at the i-th Monte-Carlo run. RMSEs in velocity can also be written similar to the position RMSEs.

1) CASE 1: UNKNOWN PROCESS AND MEASUREMENT NOISES

In a practical system, the process and measurement noises are unknown and vary with different environments as well. For the purpose of analyzing the disturbances of the unknown noises on the state estimate, the actual process noise covariance was magnified to 100 times in the time interval (50, 75) and the actual measurement noise covariance was magnified to 10 times in the time interval (100, 125), i.e.

$$\mathbf{Q}_k = \begin{cases} \mathbf{Q} & k \leqslant 50 \\ 100 * \mathbf{Q} & 50 < k \leqslant 75 \\ \mathbf{Q} & 75 < k \leqslant 200 \end{cases} \tag{80}$$

$$\mathbf{R}_k = \begin{cases} \mathbf{R} & k \leqslant 100 \\ 10 * \mathbf{R} & 100 < k \leqslant 125 \\ \mathbf{R} & 125 < k \leqslant 200 \end{cases} \tag{81}$$

In this section, the noises in the filtering are respectively set as zero means and variances $\mathbf{Q}$ and $\mathbf{R}$ in the estimation process, and the simulation time is 200s. Fig. 4 shows the RMSEs of filters under 100 Monte Carlo runs. From this figure, the RMSEs of FHKF, UHKF and AUKF after filtering stabilization are (5.51m, 4.58m/s, 0.102), (5.61m, 4.55m/s, 0.097) and (5.72m, 4.56m, 0.094), which are higher than those of UKF (7.07m, 6.45m/s, 0.127) and EHKF (7.01m, 6.21m/s, 0.126). It is observed that FHKF and UHKF exceed other methods.

Fig. 5 reports the averaged RMSEs of the four filters between 50s and 75s under the process variance unknown. During the time period (50s, 75s), the filtering performances of UKF, EHKF, and AUKF are significantly disturbed by

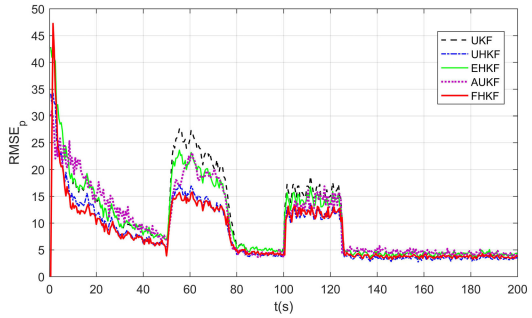

(a) RMSE in position

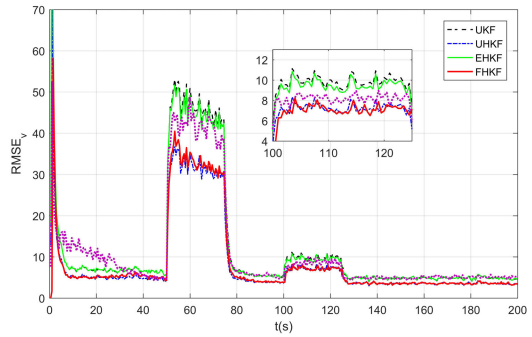

(b) RMSE in velocity

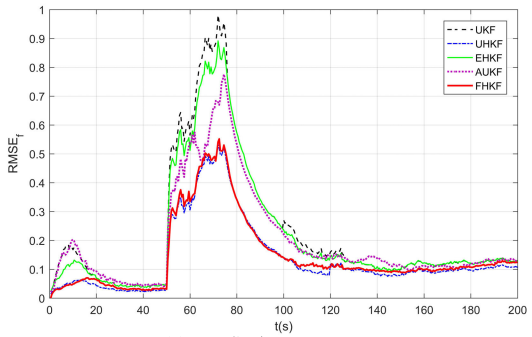

(c) RMSE in aero-param

FIGURE 4. Estimated RMSEs of different filters in case 1.

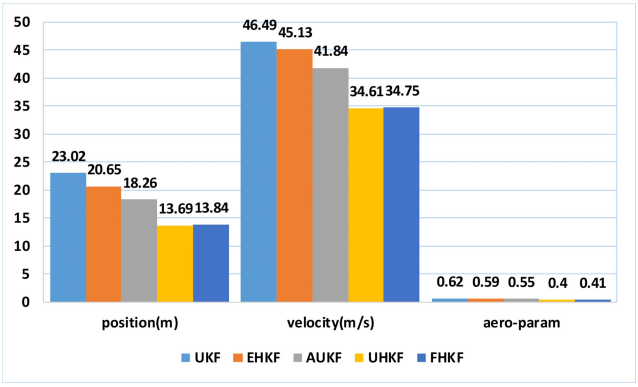

FIGURE 5. The histogram of the average RMSEs at (50s, 75s) for filters in case 1.

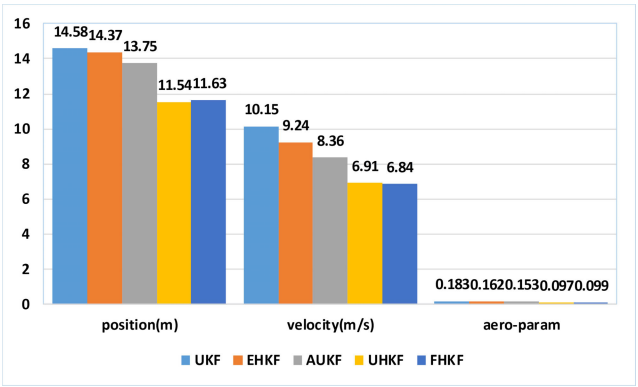

FIGURE 6. The histogram of the average RMSEs at (100s, 125s) for filters in case 1.

the biased process noise covariance, resulting in the RMSEs of (23.02m, 42.49m/s, 0.621), (20.65m, 45.13m/s, 0.617) and (18.26m, 41.84m, 0.55) respectively. Both UHKF and FHKF significantly improves the filtering performances of UKF, EHKF, and AUKF, and their RMSEs are (13.69m, 34.61m/s, 0.402), and (13.84m, 34.75m/s, 0.412) respectively. Fig. 6 shows the averaged RMSEs of four filters between 100s and 125s with the measurement variance unknown. During the time period (100s, 125s), the filtering performances of UKF, AUKF, and EHKF are significantly disturbed by the biased measurement noise covariance, resulting in the RMSEs of (14.58m, 9.15m/s, 0.163), (13.75m, 8.36m, 0.153) and (14.37m, 9.84m/s, 0.162) respectively. Both UHKF and FHKF significantly improves the filtering performances compared with UKF, AUKF, and EHKF, and their RMSEs are (11.54m, 6.91m/s, 0.097) and (11.63m, 6.84m/s, 0.099), respectively.

The time-varying results of attenuation level γ during the last Monte-Carlo run in case 1 is shown in Fig. 7. The estimated value of γ in FHKF within $(0.029, 0.633)$ stabilizes around 0.039 after 20s, while it is eventually increased to 0.198 due to the unknown noises during the time period (50s, 75s) and (100s, 125s), as shown in Fig. 4 and 7. There is an asymptotic optimal upper bound $\hat{\gamma}^2_{k,o}$ at each moment in the FHKF. Nevertheless, the value of γ in EHKF is fixed at 3.33, which is not the optimal upper bound to the total process. Combining simulation and the result in Fig. 7, the estimation process with fixed γ as EHKF can be interrupted, when the selection of fixed γ is less than $\gamma_{\max} = 0.633$. The fixed γ solution also causes the instability of the filtering process. Further, since it is not the optimal bound of filtering, the parameter γ_k in UHKF is larger than the value of FHKF from Fig. 7. The fixed η which does not advocate the optimal parameters eventually makes divergence of attenuation level of UHKF, and then leads to the poor robust, stability and availability of estimation. By contrast, from Fig. 7 the adaptive relevant parameter η_k has been designed in FHKF to ensure the asymptotic optimality of $\hat{\gamma}_{o,k}$, which takes the asymptotically optimal upper bound. Based on the analyses,

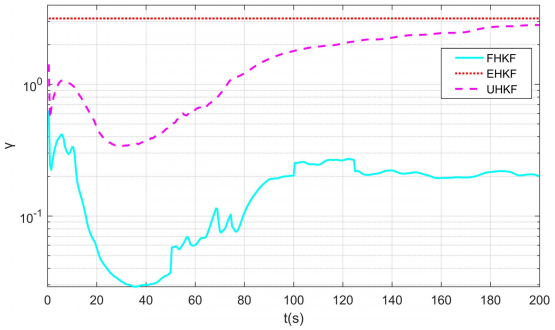

FIGURE 7. Time-varying results of γ in case 1.

the FHKF is robust to the case of unknown system noise statistics, and its precision is higher than UKF, EHKF, and AUKF. The attenuation level adaptation for FHKF is taken to improve the performance of the fixed γ solution. Meanwhile, its robustness and availability are better than UHKF by adding the adaptive tune of η_k.

2) CASE 2: ROBUST TO DYNAMICAL MODEL WITH UNCERTAIN TERM

Due to aging processes and many other unknown factors, the practical system has presented the variation compared with the dynamical model. That means there are uncertain terms in the dynamical model. In this section, the performance of the proposed FHKF is evaluated with uncertain terms in the system model. Assume that there is the unknown random term $\Delta \boldsymbol{x}_k \times rand(k)$ at (0s, 100s) in practical system, where $\Delta \boldsymbol{x}_k = [-0.1; -0.1; -0.03; -0.03; 0.01]$. The actual noises of state and measurement are $w_k \sim \mathcal{N}(\mathbf{0}, \mathbf{Q})$ and $v_k \sim \mathcal{N}(\mathbf{0}, \mathbf{R})$, respectively. The noise covariances in filtering are set as $\mathbf{Q}$ and $\mathbf{R}$.

Fig. 8 indicates the RMSEs of filters with a random uncertain term in system model by 100 Monte Carlo runs. As far as stability is concerned, the stability of FHKF outbalances to the other methods. The convergence of FHKF is faster than UKF, EHKF, and AUKF. To more clearly illustrate, the average RMSEs at (0s, 100s) and (100s, 200s) are calculated and shown in Fig. 9 and 10, respectively. Comparing Fig. 9 and 10, it is obvious that the performance of all four filters can be reduced since the model is interfered by the random uncertain term. By observing Fig. 8-9, the filtering performances of UKF, EHKF and AUKF are significantly disturbed by the random uncertain term, resulting in (38.66m, 94.43m, 0.802), (35.93m, 94.84m, 0.788) and (32.71m, 90.85m, 0.591), respectively. During the time period (0s, 100s), the precision of FHKF is higher than the above filters and close to UHKF. By observing Fig. 8 and 10, the performance of FHKF is close to UHKF without the random uncertain term during the time period (100s, 200s), which is slightly higher than other filters. On balance, compared with the Kalman-based filters, FHKF is a robust approach due to increase the use of fresh measurement, which is suitable for the estimation in case 2. It demonstrates that the FHKF has more robust than the Kalman-based filters in case 2, which inherits the advantages of H∞-based filters.

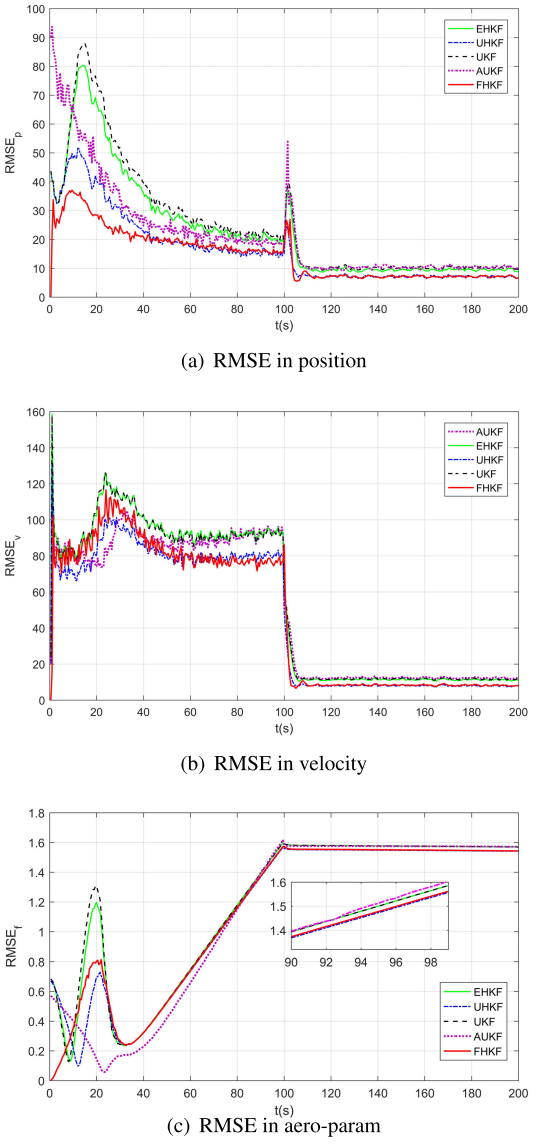

FIGURE 8. Estimated RMSEs of different filters in case 2.

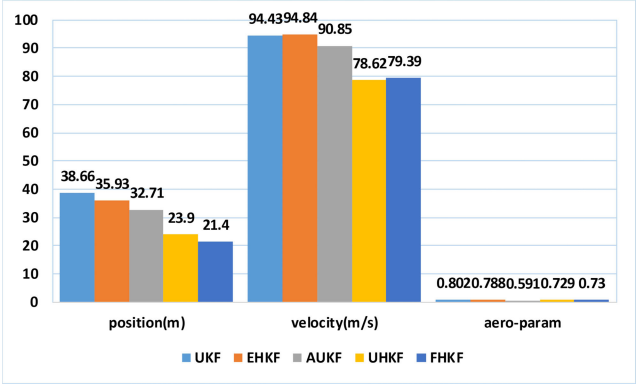

FIGURE 9. The histogram of the average RMSEs at (50s, 75s) for filters in case 2.

The time-varying results of attenuation level γ_o by the last Monte-Carlo run in case 2 is shown in Fig. 11. It is

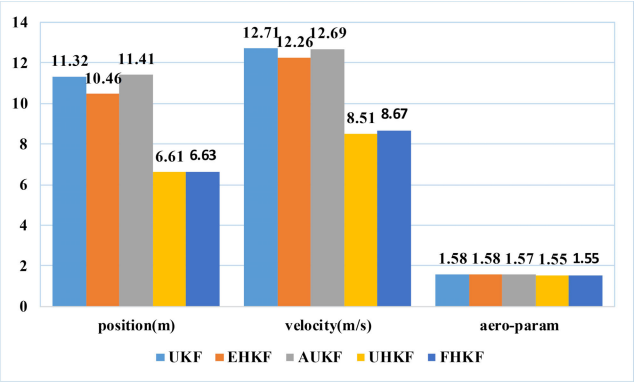

FIGURE 10. The histogram of the average RMSEs at (100s, 125s) for filters in case 2.

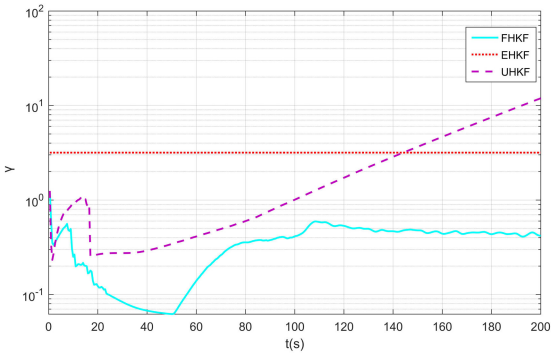

FIGURE 11. Time-varying results of γ in case 2.

evident that its estimation value in FHKF is within (0.063, 1.248), which has a rapid change at the first 100s with the influence of system uncertainty, and then it remains stable at 0.454 after 100s without the influence of system uncertainty. Moreover, the attenuation level in FHKF is increasing from 50s to 100s to reduce the impact of uncertainty. By observing Fig. 8 and 11, the RMSEs of states have been stabilized around the fixed value during the time period (50s, 100s). The value of γ in EHKF is also fixed at 3.33, which is not the optimal upper bound during the whole filtering. If it is smaller than $\gamma_{\max} = 1.248$, the malfunction of EHKF has occurred during the estimation process. The fixed γ can result in the instability of the system estimation. Moreover, the attenuation level in UHKF is not the optimal upper bound, which is larger than the value of FHKF from Fig. 11. Its curve is divergent, leading to the poor robust and availability of filtering. The robustness in UHKF is becoming worse and worse with time, and once there is uncertainty in the system, the filtering owns poor stability, or even divergence. By contrast, adaptive regulation of attenuation level in FHKF is to modify the whole performance of the other solutions as EHKF or UHKF. Our proposed FHKF outperforms all other approaches, yielding accurate state estimation in different situations.

3) COMPUTATIONAL PERFORMANCE

The computational performance of the proposed FHKF for the Reentry vehicle tracking system was evaluated with the above simulation cases. The simulations in the previous section were carried out on a Core i5 PC with 2.3-GHz CPU and 8-GB memory. The averaged computation time of UKF, EHKF, AUKF, UHKF, and FHKF for 500 steps are shown in Table 3. As can be seen from Table 3, the computation time of EHKF, UKF and AUKF are lower than FHKF, but their precision is not satisfied in the previous cases. The precisions of FHKF and UHKF are superior to the above methods. However, the robust, availability and stability of FHKF is far superior to UHKF due to its adaptive estimation of attenuation level. Meanwhile, the computation of trajectory estimation using FHKF is faster than UHKF.

TABLE 3. The average running time for different methods.

Cases	EHKF	UKF	AUKF	UHKF	FHKF
Case 1(ms)	74.60	85.46	86.34	104.69	96.63
Case 2(ms)	74.69	85.54	86.42	104.82	96.32

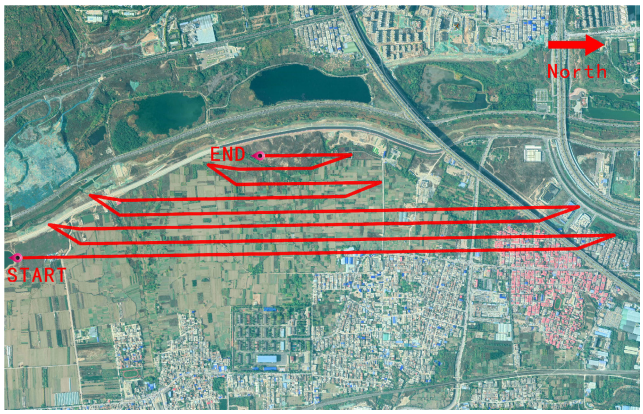

FIGURE 12. The UAV trajectory.

TABLE 4. Experiments parameters.

Initial position	East longitude	109.051°
	North latitude	34.180°
	Altitude	652m
Initial velocity	East	1m/s
	North	18 m/s
	Up	0m/s
Initial attitude	Pitch	$-5.28°$
	Roll	6.43°
	Yaw	14.59°
Initial position error	East longitude	5m
	North latitude	5m
	Altitude	5m
Initial velocity error	East	0.2 m/s
	North	0.2m/s
	Up	0.4 m/s
Initial attitude error	Pitch	0.3°
	Roll	0.3°
	Yaw	0.5°
Gyro parameters	In-run bias stability	$0.05°/s$
	Resolution	$0.0076°/s$
Accelerometer parameters	In-run bias stability	$0.01g$
	Resolution	$6.1 \times 10^{-5}g$
GPS parameters	Horizontal position error	5∼10m
	Altitude error	<15m
	Sampling frequency	1Hz

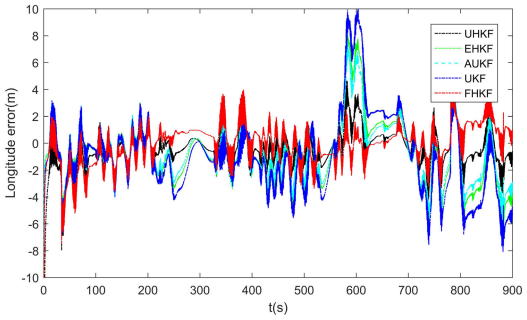

(a) Longitude error

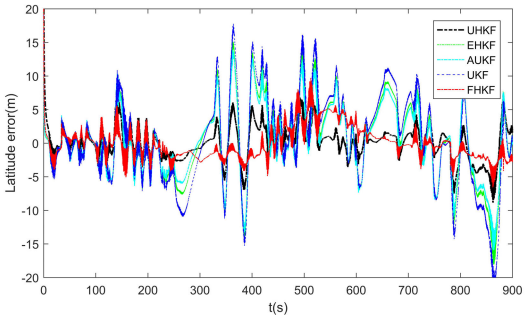

(b) Latitude error

FIGURE 13. The positions errors obtained by different filters for the UAV navigation case.

C. EXPERIMENT AND ANALYSIS

For the performance evaluation of the proposed FHKF, a practical experiment was also conducted to observe a UAV (Unmanned Aerial Vehicle) navigation in Xi′an, Shaanxi, China. The UAV applied an INS/GPS integrated system for navigation and location, and its model system can be reference literature [40]. The INS/GPS integrated system consists of an MPU 9250 inertial measurement unit (IMU) and a geom8 GPS. The position data (its precision is less than 0.1m) obtained off-line calibration of the camera (SONY ILCE-7R) with the ground control points was taken as the reference values to evaluate the position errors of UAV navigation. The sampling frequencies of IMU, GPS and camera were set to 10Hz, 1Hz, and 1Hz, respectively, and test period was 900s. The UAV trajectory is shown in Fig. 12. The parameter settings of INS/GPS integrated system were displayed in Table 4

Fig. 13 indicates the position errors of UAV by UKF, EHKF, AUKF, UHKF, and FHKF with period time 900s. During the testing process, the system noise statistics involve uncertainties due to disturbances in the dynamic environment. The UKF is significantly disturbed by the uncertainties of system noise statistics, resulting in the large magnitude of oscillations in the filtering curve. Its position errors are within (−8.12m, 10.08m) and (−22.33m, 17.75m). These are slightly larger than those obtained by EHKF, which are within (−7.76m, 8.30m) and (−18.08m, 15.12m). Due to the adding of noise estimation, the precision of AUKF is within (−7.54m, 7.88m) and (−13.45m, 13.82m), which is better than the above two filters. However, obvious oscillations still remain in the filtering curve of AUKF. In contrast, the position errors of UHKF are within (−7.32m, 4.96m) and (−6.98m, 9.42m). Meanwhile, the position errors by the proposed FHKF are within (−7.12m, 4.86m) and (−6.59m, 9.61m), which are close to UHKF. They are much smaller than those by the UKF, EHKF, and AUKF. The mean absolute errors (MAEs) and standard deviations (STDs) of the position errors by UKF, EHKF, AUKF, UHKF, and FHKF are listed in Table 5. It can be seen that the MAE and STD of the position errors of the proposed FHKF and UHKF are also much smaller than the other three methods.

TABLE 5. MAE and STD of the position errors by four filters for the UAV navigation.

Filtering methods		position	
		longitude	latitude
UKF	MAE(m)	2.1302	5.2989
	STD(m)	3.0032	6.8114
EHKF	MAE(m)	1.7334	4.3811
	STD(m)	2.4086	5.6210
AUKF	MAE(m)	1.5563	3.9783
	STD(m)	2.1543	5.0750
UHKF	MAE(m)	1.0701	1.8813
	STD(m)	1.4993	2.3862
FHKF	MAE(m)	1.0709	1.8326
	STD(m)	1.4977	2.3622

VI. CONCLUSION

In this paper, the FHKF is proposed as a derivative-free nonlinear HâĹđ filter based on numerical approximation with low computational cost. The contribution of this paper is that the novel fitting transformation is presented as a new numerical approximation technique, and then combined with EHKF to handle nonlinear uncertain systems. Meanwhile, its adaptive attenuation level is solved to improve the robustness, availability, and stability of estimation process, which is better than the other scheme as EHKF or UHKF. It gives the optimal lower bound of attenuation level in the previous scenarios and then provides a local optimal upper bound at each step time as well, which serves to select the global optimal upper bound. Moreover, the stability analysis of FHKF is presented according to the stochastic stability lemma. It's shown that the proposed method is bounded and stable regardless of the value of. Simulations and experiments show that the proposed FHKF has better precision than UKF, EHKF, and AUKF with unknown terms for nonlinear systems. Due to the proposed filter no need to compute complex Jacobian matrices manually, it is more simple than the standard EKF and EHKF. Compared with UKF and AUKF, it is robust to the system uncertainties since the use of the upper bound. Hence it is suitable for systems with unknown priori noise statistics or the uncertainty system.

APPENDIXES

APPENDIX A

$\gamma_o^2 \to \infty$, (28) can be written as

$$\mathbf{P}_k^{-1} = \mathbf{P}_{k/k-1}^{-1} + \hat{\mathbf{H}}_k^T \mathbf{R}_{k,o}^{-1} \hat{\mathbf{H}}_k \tag{82}$$

By the matrix inversion lemma and (82), there is

$$\begin{aligned}\mathbf{P}_k &= \mathbf{P}_{k/k-1} - \mathbf{P}_{k/k-1}\hat{\mathbf{H}}_k^T(\mathbf{R}_{k,o} + \hat{\mathbf{H}}_k\mathbf{P}_{k/k-1}\hat{\mathbf{H}}_k^T)^{-1} \\ &\quad \times \hat{\mathbf{H}}_k\mathbf{P}_{k/k-1} \\ &= \mathbf{P}_{k/k-1} - \mathbf{K}_k\hat{\mathbf{H}}_k\mathbf{P}_{k/k-1} \\ &= \mathbf{P}_{k/k-1} - \mathbf{K}_k(\mathbf{R}_{k,o} + \hat{\mathbf{H}}_k\mathbf{P}_{k/k-1}\hat{\mathbf{H}}_k^T)\mathbf{K}_k \end{aligned} \tag{83}$$

Therefore, when $\gamma_o^2 \to \infty$, (19)-(24) and (83) in FHKF are equal to the linear fitting Kalman in [31] (24)-(34).

APPENDIX B

Consider a nonlinear function $z = g(\boldsymbol{x})$ evaluated in $2n$ sigma points, i.e., $(\boldsymbol{x}_i, z_i)$, where $z_i = g(\boldsymbol{x}_i)$ for $i = 1, \cdots, 2n$. Assuming that the nonlinear function is statistically linearized as (3), which is

$$z = \mathbf{A}\boldsymbol{x} + \boldsymbol{b} + \boldsymbol{e} = \tilde{\mathbf{A}}\tilde{\boldsymbol{x}} + \boldsymbol{e} \tag{84}$$

The objective of fitting transformation is to find $\hat{\tilde{\mathbf{A}}}$ so that the point-wise linearization error $\boldsymbol{e}_i$ is minimized, i.e.,

$$\hat{\tilde{\mathbf{A}}} = arg\ min \sum_{i=1}^{2n} \boldsymbol{w}_i \boldsymbol{e}_i^T \boldsymbol{e}_i \tag{85}$$

where $\hat{\tilde{\mathbf{A}}} = [\hat{\mathbf{A}}, \hat{\boldsymbol{b}}]$, and $\boldsymbol{e}_i = z_i - \tilde{\mathbf{A}}\tilde{\boldsymbol{x}}_i = z_i - (\mathbf{A}\boldsymbol{x}_i + \boldsymbol{b})$. By taking the derivative of (85) with respect to $\tilde{\mathbf{A}}$, then let it equal to zero, that is $\mathbf{Z} = \tilde{\mathbf{A}}\tilde{\mathbf{X}}$, as the system model Eq. (14), which is transformed to

$$\mathbf{A}\hat{\tilde{X}}W\tilde{\mathbf{X}}^T = \mathbf{Z}\mathbf{W}\tilde{\mathbf{X}}^T \tag{86}$$

where $\tilde{\mathbf{X}}$ and $\mathbf{W}$ can be set as FT in table 1. Substitute $\hat{\tilde{\mathbf{A}}} = [\hat{\mathbf{A}}, \hat{\boldsymbol{b}}]$ into (86) for decomposition, and obtain

$$\hat{\boldsymbol{b}} = \bar{z} - \hat{\mathbf{A}}\bar{\boldsymbol{x}} \tag{87}$$

where $\bar{\boldsymbol{x}} = \sum_{i=1}^{2n} \boldsymbol{w}_i\boldsymbol{x}_i$ and $\bar{z} = \sum_{i=1}^{2n} \boldsymbol{w}_i f(\boldsymbol{x}_i) = \sum_{i=1}^{2n} \boldsymbol{w}_i z_i$. Next, the error covariance of parameter estimation is written as

$$\begin{aligned}\mathbf{P}_{ee} &= \sum_{i=1}^{2n} \boldsymbol{w}_i\hat{\boldsymbol{e}}_i\hat{\boldsymbol{e}}_i^T \\ &= \sum_{i=1}^{2n} \boldsymbol{w}_i[z_i - \hat{\tilde{\mathbf{A}}}\tilde{\boldsymbol{x}}_i][*]^T \\ &= \sum_{i=1}^{2n} \boldsymbol{w}_i[z_i - (\hat{\mathbf{A}}\boldsymbol{x}_i + \hat{\boldsymbol{b}})][*]^T \\ &= \sum_{i=1}^{2n} \boldsymbol{w}_i[z_i - \hat{\mathbf{A}}\boldsymbol{x}_i + \hat{\mathbf{A}}\bar{\boldsymbol{x}} - \bar{z})][*]^T \\ &= \sum_{i=1}^{2n} \boldsymbol{w}_i[z_i - \bar{z}][*]^T - \hat{\mathbf{A}}\mathbf{P}_{xx}\hat{\mathbf{A}}^T \end{aligned} \tag{88}$$

Then, by taking the expectation and the outer product of fitting transformation, respectively, the posterior statistics are given by

$$\begin{aligned}\hat{z} &= \hat{\mathbf{A}}\bar{\boldsymbol{x}} + \hat{\boldsymbol{b}} \\ &= \hat{\mathbf{A}}\bar{\boldsymbol{x}} + (\bar{z} - \hat{\mathbf{A}}\bar{\boldsymbol{x}}) \\ &= \sum_{i=1}^{2n} \boldsymbol{w}_i z_i \\ \mathbf{P}_{zz} &= \hat{\mathbf{A}}\mathbf{P}_{xx}\hat{\mathbf{A}}^T + \mathbf{P}_{ee} \\ &= \hat{\mathbf{A}}\mathbf{P}_{xx}\hat{\mathbf{A}}^T + \sum_{i=1}^{2n} \boldsymbol{w}_i[z_i - \bar{z}][*]^T - \hat{\mathbf{A}}\mathbf{P}_{xx}\hat{\mathbf{A}}^T \\ &= \sum_{i=1}^{2n} \boldsymbol{w}_i[z_i - \bar{z}][*]^T \end{aligned} \tag{89}$$

where is the same expression as UT to the nonlinear function $z = g(\boldsymbol{x})$, which means that its precision is in accord with the UT.

REFERENCES

[1] M. Mertens, M. Ulmke, and W. F. Koch, "Ground target tracking with RCS estimation based on signal strength measurements," *IEEE Trans. Aerosp. Electron. Syst.*, vol. 52, no. 1, pp. 205–220, Apr. 2016.

[2] G. Wang, N. Li, and Y. Zhang, "Maximum correntropy unscented Kalman and information filters for non-Gaussian measurement noise," *J. Franklin Inst.*, vol. 354, no. 18, pp. 8659–8677, Oct. 2017.

[3] E. Ghorbani and Y. J. Cha, "An iterated cubature unscented Kalman filter for large-DoF systems identification with noisy data," *J. Sound Vib.*, vol. 420, pp. 21–34, Apr. 2018.

[4] S. Dan, *Optimal State Estimation: Kalman, H-Infinity, and Nonlinear Approaches*. Hoboken, NJ, USA: Wiley, 2006, pp. 343–354.

[5] A. Taghvaei, J. D. Wiljes, and P. G. Mehta, "Kalman filter and its modern extensions for the continuous-time nonlinear filtering problem," *J. Dyn. Syst., Meas., Control*, vol. 140, no. 3, pp. 1–24, Mar. 2018.

[6] Y. Y. Chen, Y. Zhang, and C. L. Liu, "Formation circumnavigation for unmanned aerial vehicles using relative measurements with an uncertain dynamic target," *Nonlinear Dyn.*, vol. 29, no. 4, pp. 2305–2321, Jul. 2019.

[7] Y. Y. Chen, X. Ai, and Y. Zhang, "Spherical formation tracking control for second-order agents with unknown general flowfields and strongly connected topologies," *Int. J. Robust Nonlinear Control*, vol. 29, pp. 3715–3736, Feb. 2019.

[8] B. K. Kwon and S. Han, "A robust extended Kalman filtering for linearization errors," in *Proc. Int. Conf. Control, Autom. Syst.*, Busan, South Korea, Oct. 2015, pp. 1485–1487.

[9] K. D. Sebesta and N. Boizot, "A real-time adaptive high-gain EKF, applied to a quadcopter inertial navigation system," *IEEE Trans. Ind. Electron.*, vol. 61, no. 1, pp. 495–503, Jan. 2014.

[10] G. G. Hu and S. S. Gao, "Stochastic stability of the derivative unscented Kalman filter," *Chin. Phys. B*, vol. 24, no. 7, pp. 64–73, Jul. 2015.

[11] B. Gao, S. Gao, Y. Zhong, G. Hu, and C. Gu, "Interacting multiple model estimation-based adaptive robust unscented Kalman filter," *Int. J. Control, Automat. Syst.*, vol. 15, no. 5, pp. 2013–2025, Jul. 2017.

[12] I. Arasaratnam and S. Haykin, "Cubature Kalman filters," *IEEE Trans. Autom. Control*, vol. 54, no. 6, pp. 1254–1269, Jun. 2009.

[13] J. Zhang, S. Gao, and Y. Zhong, "An advanced cubature information filtering for indoor multiple wideband source tracking with a distributed noise statistics estimator," *IEEE Access*, vol. 7, p. 1, 2019.

[14] R. Astroza, H. Ebrahimian, and J. P. Conte, "Performance comparison of Kalman-based filters for nonlinear structural finite element model updating," *J. Sound Vib.*, vol. 438, pp. 520–542, Jan. 2019.

[15] K. V. Yuen and S. C. Kuok, "Bayesian methods for updating dynamic models," *Appl. Mech. Rev.*, vol. 64, no. 1, pp. 3–7, Jan. 2011.

[16] L. Cheng, X. Gong, and X. Rui, "A novel H-infinity and EKF joint estimation method for determining the center of gravity position of electric vehicles," *Appl. Energy*, vol. 194, pp. 609–616, May 2017.

[17] Z. Mattia, "Robust Kalman filtering under model perturbations," *IEEE Trans. Autom. Control*, vol. 62, no. 6, pp. 2902–2907, Aug. 2016.

[18] L. Cao, W. W. Yang, and H. N. Li, "Robust double gain unscented Kalman filter for small satellite attitude estimation," *Adv. Space Res.*, vol. 60, no. 3, pp. 499–512, Mar. 2017.

[19] X. Chang and G. H. Yang, "Robust H-infinity filtering for uncertain discrete-time systems using parameter-dependent Lyapunov functions," *Control Theory Technol.*, vol. 11, no. 1, pp. 122–127, Jan. 2013.

[20] J. Zhao and L. Mili, "A decentralized H-infinity unscented Kalman filter for dynamic state estimation against uncertainties," *IEEE Trans. Smart Grid*, vol. 10, no. 5, pp. 4870–4880, Sep. 2018.

[21] C. E. de Souza, "Robust H-infinity filtering for a class of discrete-time Lipschitz nonlinear systems," *Automatica*, vol. 103, pp. 69–80, May 2019.

[22] M. Charkhgard and M. H. Zarif, "Design of adaptive H-infinity filter for implementing on state-of-charge estimation based on battery state-of-charge-varying modelling," *IET Power Electron.*, vol. 8, no. 10, pp. 1825–1833, Sep. 2015.

[23] G. B. Koo, J. B. Park, and Y. H. Joo, "Sampled-data H-infinity fuzzy filtering for nonlinear systems with missing measurements," *Fuzzy Sets Syst.*, vol. 316, pp. 82–98, Jun. 2016.

[24] A. L'Afflitto, "Differential games, continuous Lyapunov functions, and stabilisation of non-linear dynamical systems," *IET Control Theory Appl.*, vol. 11, no. 15, pp. 2486–2496, Sep. 2017.
[25] J. B. Zhao, "Dynamic state estimation with model uncertainties using H-infinity extended Kalman filter," *IEEE Trans. Power Syst.*, vol. 33, no. 1, pp. 1099–1100, Mar. 2018.
[26] K. P. B. Chandra, D. W. Gu, and I. Postlethwaite, "Fusion of an extended H-infinity filter and cubature Kalman filter," *IFAC Proc. Volumes*, vol. 44, no. 1, pp. 9091–9096, Jan. 2011.
[27] M. Zhong, D. Guo, and D. Zhou, "A krein space approach to H-infinity filtering of discrete-time nonlinear systems," *IEEE Trans. Circuits*, vol. 61, no. 9, pp. 2644–2652, Sep. 2017.
[28] D. K. Bebarta, R. Bisoi, and P. K. Dash, "Locally recurrent functional link fuzzy neural network and unscented H-infinity filter for shortterm prediction of load time series in energy markets," in *Proc. Power, Commun. Inf. Technol. Conf.*, Bhubaneswar, India, Mar. 2016, pp. 663–670.
[29] H. K. Sahoo and P. K. Dash, "Robust estimation of power quality disturbances using unscented H-infinity filter," *Int. J. Electr. Power Energy Syst.*, vol. 73, pp. 438–447, Dec. 2015.
[30] W. Li and Y. Jia, "H-infinity filtering for a class of nonlinear discrete-time systems based on unscented transform," *Signal Process.*, vol. 90, no. 12, pp. 3301–3307, Dec. 2010.
[31] R. Havangi, "Unscented H-infinity filtering based simultaneous localization and mapping with evolutionary resampling," *J. Franklin Inst.*, vol. 352, no. 11, pp. 4801–4825, Dec. 2015.
[32] K. P. Chandra, D. W. Gu, and I. Postlethwaite, "A cubature H-infinity filter and its square-root version," *Int. J. Control*, vol. 87, no. 4, pp. 764–776, Apr. 2014.
[33] K. P. Chandra, D. W. Gu, and I. Postlethwaite, "Cubature H-infinity information filter and its extensions," *Eur. J. Control*, vol. 29, pp. 17–32, Mar. 2016.
[34] J. Xia, S. Gao, B. Gao, W. Wei, and T. Tian, "Fitting H-infinity filter for nonlinear discrete-time systems," in *Proc. Chin. Control Decis. Conf.*, Nanchang, China, 2019, pp. 4022–4027.
[35] Y. Xiong and X. Zhong, "Linear fitting Kalman filter," *IET Signal Process.*, vol. 10, no. 4, pp. 404–412, Jun. 2016.
[36] B. Xu, P. Zhang, H. Z. Wen, and X. Wu, "Stochastic stability and performance analysis of cubature Kalman filter," *Neurocomputing*, Nanchang, China, vol. 186, pp. 218–227, Jan. 2017.
[37] S. Y. Wang and W. L. Wang, "Convergence analysis of nonlinear Kalman filters with novel innovation-based method," *Neurocomputing*, vol. 289, pp. 188–194, May 2018.
[38] L. Chang, B. Hu, A. Li, and F. Qin, "Transformed unscented Kalman filter," *IEEE Trans. Autom. Control*, vol. 58, no. 1, pp. 252–257, Jan. 2013.
[39] S. Peng, C. Chen, H. Shi, and Z. Yao, "State of charge estimation of battery energy storage systems based on adaptive unscented Kalman filter with a noise statistics estimator," *IEEE Access*, vol. 5, pp. 13202–13212, 2017.
[40] B. B. Gao and S. S. Gao, "Maximum likelihood principle and moving horizon estimation based adaptive unscented Kalman filter," *Aerosp. Sci. Technol.*, vol. 73, pp. 184–196, Dec. 2017.

JUAN XIA is currently pursuing the Ph.D. degree with the School of Automatics, Northwestern Polytechnical University, China. Her research interests include control theory and engineering, navigation, guidance and control, optimum estimation and control, information fusion, target tracking, and integrated navigation.

SHESHENG GAO is currently a Professor with the School of Automatics, Northwestern Polytechnical University, China. His research interests include control theory and engineering, navigation, guidance and control, optimum estimation and control, integrated inertial navigation systems, and information fusion.

YONGMIN ZHONG is currently a Senior Lecturer with the School of Aerospace, Mechanical and Manufacturing Engineering, RMIT University, Australia. His research interests include virtual reality and haptics, soft tissue modeling and surgery simulation, robotics, mechatronics, optimum estimation and control, and integrated navigation systems.

JIAHAO ZHANG is currently pursuing the Ph.D. degree with the School of Automatics, Northwestern Polytechnical University, China. His research interests include control theory and engineering, navigation, guidance and control, target tracking, signal processing, and information fusion.

CHENGFAN GU is currently an ARC DECRA Fellow with the School of Aerospace, Mechanical and Manufacturing Engineering, RMIT University, Australia. Her current research activity includes computational modeling, micro/nano manufacturing, fatigue and bio/nano mechanics, and advanced materials characterization.

YANG LIU received the master's degree from the East China University of Technology, in 2017. He is currently working with the Research Institute of Mechanical Industry Survey and Design Limited, where he is responsible for UAV aerial photogrammetry. His research interests include computer vision and UAV aerial survey.